

1 **August 12, 2021**

2

3 **Toxoplasma bradyzoites exhibit physiological plasticity of calcium and energy**
4 **stores controlling motility and egress.**

5

6 Yong Fu¹, Kevin M. Brown^{1a}, Nathaniel G. Jones^{1b}, Silvia N. J. Moreno², L. David Sibley^{1*}

7 ¹Department of Molecular Microbiology, Washington University in St. Louis, School of Medicine, St Louis,
8 MO, United States

9 ²Center for Tropical and Emerging Global Diseases and Department of Cellular Biology, University of
10 Georgia, Athens, GA, United States

11

12 Running title: *Calcium signaling in bradyzoites*

13 * Corresponding author

14 E-mail: sibley@wustl.edu

15

16 Present addresses

17 ^aDepartment of Microbiology and Immunology, University of Oklahoma Health Sciences Center, College of
18 Medicine, Oklahoma City, OK, United States

19 ^bYork Biomedical Research Institute, Department of Biology, University of York, Wentworth Way, Heslington,
20 York, YO10 5DD, U.K.

21

22 **Key words:** tissue cyst, chronic infection, microneme secretion, calcium signaling, calcium ATPases,
23 exocytosis, motility, dormancy, latency, reactivation

24

25

26

27 **Abstract**

28 *Toxoplasma gondii* has evolved different developmental stages for disseminating during acute infection (i.e.
29 tachyzoites) and for establishing chronic infection (i.e. bradyzoites). Calcium ion (Ca^{2+}) signaling tightly
30 regulates the lytic cycle of tachyzoites by controlling microneme secretion and motility to drive egress and
31 cell invasion. However, the roles of Ca^{2+} signaling pathways in bradyzoites remain largely unexplored. Here
32 we show that Ca^{2+} responses are highly restricted in bradyzoites and that they fail to egress in response to
33 agonists. Development of dual-reporter parasites revealed dampened calcium responses and minimal
34 microneme secretion by bradyzoites induced in vitro or harvested from infected mice and tested ex vivo.
35 Ratiometric Ca^{2+} imaging demonstrated lower Ca^{2+} basal levels, reduced magnitude, and slower Ca^{2+} kinetics
36 in bradyzoites compared with tachyzoites stimulated with agonists. Diminished responses in bradyzoites were
37 associated with down-regulation of calcium ATPases involved in intracellular Ca^{2+} storage in the endoplasmic
38 reticulum (ER) and acidocalcisomes. Once liberated from cysts by trypsin digestion, bradyzoites incubated in
39 glucose plus calcium rapidly restored their intracellular Ca^{2+} and ATP stores leading to enhanced gliding.
40 Collectively, our findings indicate that intracellular bradyzoites exhibit dampened Ca^{2+} signaling and lower
41 energy levels that restrict egress, and yet upon release they rapidly respond to changes in the environment to
42 regain motility.

43

44 **Introduction**

45 *Toxoplasma gondii* is an obligate intracellular parasite, capable of infecting nearly all warm-blooded
46 animals and frequently causing human infections [1]. The ingestion of tissue cysts in undercooked meat or
47 shed oocysts by infected cats are the major transmission routes of *T. gondii* [2,3]. Following oral ingestion of
48 bradyzoites within tissue cysts or sporozoites within oocysts, the parasite migrates across the intestinal
49 epithelial barrier and disseminates throughout the body as the actively proliferating tachyzoite form that
50 infects many cell types but primarily traffics in monocytes [4]. In response to immune pressure, the parasite
51 differentiates to asynchronously growing bradyzoites within cysts that can persist as chronic infections in
52 muscle and brain tissues [5-7].

53 Tachyzoites are adapted for rapid proliferation and dissemination due to an active lytic cycle that is
54 controlled at numerous stages by intracellular calcium ion (Ca^{2+}) signaling [8]. Artificially elevating
55 intracellular Ca^{2+} using ionophores triggers secretion of microneme proteins, which are needed for substrate
56 and cell attachment, and hence critical for both gliding motility and cell invasion [9-11]. Increase of cytosolic
57 Ca^{2+} released from internal stores is sufficient to trigger microneme secretion [12], and necessary for host cell
58 invasion [12,13], although these processes are also enhanced by the presence of extracellular Ca^{2+} [14].
59 Increases in intracellular Ca^{2+} also precede egress and drive secretion of perforin like protein 1 (PLP1) from
60 microneme to facilitate rupture of parasitophorous vacuole membrane (PVM) followed by egress [15].
61 Calcium signaling is initiated by cyclic guanosine monophosphate (cGMP)-generating guanylate cyclase (GC)
62 [16-18] that activates parasite plasma membrane-associated protein kinase G (PKG) [19], stimulating the
63 production of inositol triphosphate (IP_3) by phosphoinositide-phospholipase C (PI-PLC) and leading to
64 subsequent release of intracellular Ca^{2+} [12,20,21]. Recent studies in *Plasmodium* also implicate PKG in
65 directly controlling calcium through interaction with a multimembrane spanning protein that may function as

66 a channel that mediates calcium release [22]. In turn, Ca^{2+} activates downstream Ca^{2+} responsive proteins
67 including Ca^{2+} dependent protein kinases such as CDPK1 [8] and CDPK3 [23,24], and C2 domain-containing
68 Ca^{2+} binding proteins [25], and calcium binding orthologues of calmodulin [26], which are required for
69 invasion and egress by tachyzoites. Following invasion, protein kinase A catalytic domain 1 (PKAc1)
70 dampens cytosolic Ca^{2+} by suppressing cGMP signaling and reducing Ca^{2+} uptake [27,28]. Collectively, the
71 lytic life cycle of tachyzoites is orchestrated spatially and temporally by controlling levels of intracellular Ca^{2+}
72 and cyclic nucleotides [29].

73 *Toxoplasma* has evolved elaborate mechanism to control intracellular Ca^{2+} levels through the concerted
74 action of calcium channels, transporters, and Ca^{2+} pumps expressed at the PM and intracellular stores [8,30].
75 Orthologues to voltage-dependent Ca^{2+} channels, transient receptor potential (TRP) channels, and plasma
76 membrane type Ca^{2+} -ATPases (PMCA) are predicted to be present in *T. gondii* and likely involved in
77 regulating cytosolic Ca^{2+} influx and efflux [31,32]. The endoplasmic reticulum (ER) is the most important
78 storage site from which Ca^{2+} is released to stimulate motility and egress of *Toxoplasma* [8]. SERCA-type Ca^{2+}
79 ATPase is the known mechanism for Ca^{2+} uptake by the ER and its activity, which is inhibited by thapsigargin
80 [33], leads to accumulation of Ca^{2+} in the ER, which when released activates microneme secretion and
81 motility [34,35]. TgA1 a plasma membrane type Ca^{2+} ATPase, transport Ca^{2+} to the acidocalcisome [36],
82 which likely provides a Ca^{2+} sink albeit one that may not be as readily mobilizable as the ER. In addition to
83 internal Ca^{2+} stores, intracellular and extracellular *T. gondii* tachyzoites are capable of taking up Ca^{2+} from
84 host cells and the extracellular environment, respectively, to enhance Ca^{2+} signaling pathways [14,37]. A
85 variety of fluorescent Ca^{2+} indicators that have been developed to directly image Ca^{2+} signals in live cells
86 include Ca^{2+} responsive dyes and genetically encoded indicators [38]. Indicators like Fluo-4/AM, and related
87 derivatives, have been previously used to monitor Ca^{2+} levels in extracellular parasites [34,39]. Genetically
88 encoded calcium indicators such as GCaMP5, GCaMP6f and GCaMP7 have also been used to visualize
89 dynamic Ca^{2+} signals of both intracellular and extracellular tachyzoites with high resolution and sensitivity
90 [37,40-42].

91 In contrast to tachyzoites, little is known about the roles of Ca^{2+} signaling in control of microneme
92 secretion, gliding motility, and egress by bradyzoites. Although bradyzoites divide asynchronously, they
93 undergo growth, expansion, and sequential rounds of tissue cyst formation and rupture that maintain chronic
94 infection in vivo [5]. Histological studies in animal models support a model of periodic cyst rupture [43],
95 releasing bradyzoites that reinvade new host cells to generate secondary daughter cysts [44], or transition back
96 to actively replicating tachyzoites [45]. Development of bradyzoites has been studied in vitro using systems
97 that induce development due to stress induced by alkaline pH [46] or in cell lines where development occurs
98 spontaneously [47,48]. Although numerous studies have focused on the determinants that control stage
99 conversion between tachyzoites and bradyzoites [6,49], few studies focus on the signaling pathways that
100 control the bradyzoite lytic cycle.

101 In the present study, we combined stage-specific bradyzoite fluorescent reporters with Ca^{2+} imaging
102 probes to explore Ca^{2+} signaling, microneme secretion, motility and egress by bradyzoites. Our findings
103 indicate that bradyzoites exhibit dampened Ca^{2+} levels, reduced microneme secretion, and minimal egress in
104 response to Ca^{2+} agonists. Ratiometric Ca^{2+} imaging demonstrated lower Ca^{2+} basal levels and significantly

105 lower stored Ca^{2+} in ER and acidocalcisome in bradyzoites, associated with reduced expression of Ca^{2+}
106 ATPases responsible for maintaining intracellular stores. Incubation of extracellular bradyzoites in Ca^{2+} plus
107 glucose lead to rapid recover of both intracellular Ca^{2+} and ATP levels and restored motility. Collectively our
108 findings support a dampened lytic cycle in bradyzoites, arising from diminished Ca^{2+} signaling and lowered
109 energy stores, and that upon release they exhibit rapid metabolic responsiveness to environmental conditions.

110

111 **Results**

112 **Ca^{2+} signaling triggers inefficient egress by bradyzoites**

113 To define egress by bradyzoites, we induced the differentiation of tachyzoites to bradyzoites by culture in
114 HFF cells at alkaline pH (8.2) for 7 days. We treated both tachyzoite cultures and in vitro differentiated cysts
115 with Ca^{2+} ionophore A23187 to trigger egress from parasitophorous vacuoles (PVs) or bradyzoite cysts, as
116 detected by indirect immunofluorescence assay (IFA) or time lapse video microscopy. We observed that
117 A23187 induced complete egress of tachyzoites from disrupted PVs while only few bradyzoites were released
118 from cysts that remained largely intact (**Figure 1A**). This result was also confirmed by time-lapse video
119 microscopy using the ME49 BAG1-mCherry strain either grown as tachyzoites (**Figure 1-video 1**) or
120 bradyzoites (**Figure 1-video 2**). We quantified the percentage of tachyzoites or bradyzoites that were released
121 during egress in response to A23187 or the agonist zaprinast, which is a cGMP specific phosphodiesterase
122 (PDE) inhibitor that activates PKG-mediated Ca^{2+} signaling, leading to egress. In contrast to tachyzoites, we
123 found significantly lower egress rate of bradyzoites in response to A23187 or zaprinast (**Figure 1B**). To
124 examine the behavior of released parasites, we determined the maximum egress distance that parasites moved
125 away from the original vacuole or cyst following egress. Tachyzoites migrated much further than bradyzoites
126 after induced egress (**Figure 1C**). Bradyzoites also moved more slowly than tachyzoites (**Figure 1D**), as
127 shown by quantification of their trajectories from time lapse video microscopy images. Taken together, these
128 findings indicate that egress by bradyzoites in response to Ca^{2+} ionophore or zaprinast is incomplete and
129 restricted.

130

131 **Calcium-mediated microneme secretion is dampened by bradyzoite development**

132 Egress by parasites requires Ca^{2+} -stimulated microneme secretion. To examine the reason for inefficient
133 egress by bradyzoites, we monitored microneme secretion by quantitative secretion analysis of MIC2 fused
134 with *Gaussia* Luciferase (Gluc). The *MIC2-Gluc* reporter was randomly integrated into the genome of the
135 BAG1-mCherry strain (**Figure 2A**). IFA revealed that MIC2-Gluc was expressed and localized to
136 micronemes in tachyzoites and bradyzoites induced for 7 days at pH 8.2 in vitro, as confirmed by expression
137 of BAG1-mCherry (**Figure 2B**). BAG1-mCherry MIC2-GLuc strain tachyzoites, and bradyzoites liberated
138 from cysts produced by cultivation for 7 days at pH 8.2 in vitro, were sorted by FACS (**Figure 2C**). FACS
139 sorted tachyzoites and bradyzoites were treated with zaprinast or ionomycin, a Ca^{2+} ionophore that induces
140 release of Ca^{2+} from the ER [50]. Bradyzoites secreted much less MIC2-Gluc protein compared to tachyzoites
141 in response to Ca^{2+} agonists, zaprinast and ionomycin as shown by *Gaussia* luciferase assays performed on
142 ESA fractions collected following stimulation (**Figure 2D**). To further investigate the process of microneme
143 secretion by bradyzoites, we randomly integrated a mCherry secretion reporter, based on the signal peptide

144 sequence of ferredoxin-NADP(+)-reductase (FNR-mCherry), into the genome of BAG1-EGFP parasites
145 (**Figure 2E**). The FNR-mCherry reporter is an improved version of DsRed reporter that is secreted into the
146 matrix of PV, and released following the discharge of PLP1 in response to Ca^{2+} agonists [15]. Then we
147 monitored the permeabilization of PV membrane or cyst wall after stimulation with A23187 based on the
148 diffusion of FNR-mCherry using time-lapse fluorescence video microscopy. Consistent with previous reports
149 [51], we observed that A23187 stimulated fast leakage of FNR-mCherry from the PV surrounding tachyzoites
150 (**Figure 2F**, top panel and **Figure 2-video 1**). However, FNR-mCherry was not released from the cyst after
151 A23187 stimulation (**Figure 2F**, middle panel and **Figure 2-video 3**). As a control to confirm that the
152 FNR-mCherry was indeed secreted into the lumen of the cyst matrix, we treated cysts with trypsin to release
153 bradyzoites. Once the cyst wall was digested, the FNR-mCherry dissipated rapidly, confirming that it was
154 present in the matrix of the cyst (**Figure 2F**, bottom panel and **Figure 2-video 2**). These data were also
155 confirmed by plotting FNR-mCherry fluorescence intensity changes vs. time for tachyzoites vs. intact or
156 trypsin treated cysts (**Figure 2G**). These findings demonstrate dampened microneme secretion by bradyzoites,
157 which may explain their incomplete egress.

158

159 **Genetically encoded calcium reporter reveals dampened Ca^{2+} responses in bradyzoites**

160 To investigate Ca^{2+} signaling in bradyzoites, we established a dual fluorescent reporter system containing
161 constitutively expressed GCaMP6f and mCherry under the control of bradyzoite stage-specific promoter
162 BAG1 (**Figure 3A**). Using this system, both tachyzoites and bradyzoites express the same levels of GCaMP6f,
163 while only bradyzoites express mCherry, allowing specific monitoring of Ca^{2+} signals in both stages. We
164 compared the response of BAG1-mCherry GCaMP6f reporter parasites that were grown as tachyzoites, to
165 those induced to form bradyzoites by cultivation in HFF cells for 7 days at pH 8.2 in vitro, after treatment
166 with Ca^{2+} ionophore A23187. A23187 induced rapid and high-level increases in GCaMP6f fluorescence in
167 tachyzoites but delayed and much weaker responses in bradyzoites as monitored by time-lapse video
168 microscopy (**Figure 3B**, **Figure 3-video 1** and **Figure 3-video 2**). To determine the effect of bradyzoite
169 development on Ca^{2+} signaling, we treated intracellular tachyzoites, vs. bradyzoites induced by cultivation in
170 HFF cells at pH 8.2 in vitro for 4 to 7 days, and quantified time of each tachyzoite vacuole or bradyzoite cyst
171 to reach Ca^{2+} peak level after addition of A23187 ionophore by video microscopy. Increasing time of
172 bradyzoites development was associated with progressively longer times to reach peak fluorescence of
173 GCaMP6f (**Figure 3C**). Time lapse recording of GCaMP6f fluorescence intensity ratio changes (F/F_0) showed
174 delayed Ca^{2+} increase and lower fold changes in bradyzoites compared with tachyzoites in response to
175 A23187 stimulation (**Figure 3D**). Zaprinast also elicited slower Ca^{2+} increases and lower fold changes in
176 bradyzoites compared with tachyzoites even in the presence of extracellular Ca^{2+} (**Figure 3E**). To better
177 characterize Ca^{2+} responses of bradyzoites, we performed live video imaging using spinning disc confocal
178 microscopy to distinguish individual bradyzoites within in vitro differentiated cysts and identify motile
179 bradyzoites within cysts by comparing consecutive images (**Figure 3F**). Motile bradyzoites were also
180 observed to have higher GCaMP6f signals and these typically oscillated over time. In response to Ca^{2+}
181 agonists, intracellular bradyzoites showed reduced percentages of motility compared to tachyzoites (**Figure**
182 **3G**). In summary, Ca^{2+} dynamics are delayed and reduced in bradyzoites in response to Ca^{2+} agonists.

183

184 **Bradyzoites formed in skeletal muscle cell and within ex vivo cysts show diminished Ca²⁺ responses**

185 To rule out the possibility that alkaline pH stress used for differentiation resulted in lowered Ca²⁺ signals in
186 bradyzoites, we examined Ca²⁺ signaling in bradyzoites within cysts that formed naturally in differentiated
187 C2C12 myocytes. Differentiated myocytes stained positively for skeletal myosin, and facilitated the
188 development of bradyzoites, as shown using the bradyzoite stage-specific protein BAG1 (**Figure 4A**). We
189 tested Ca²⁺ responses of bradyzoites formed in muscle cells using the dual fluorescent reporter GCaMP6f
190 BAG1-mCherry parasites in response to A23187 or zaprinast by time-lapse video recording. Time-lapse
191 imaging showed slow increase of GCaMP6f fluorescence in response to A23187 in tissue cysts formed in
192 C2C12 myocytes (**Figure 4B**). Both the rate of increase and the maximum amplitude of the GCaMP6f signal
193 was much lower in bradyzoites differentiated in myocytes compared to tachyzoites cultured in
194 undifferentiated myoblasts (**Figure 4C**). The time to reach the peak GCaMP6f fluorescence was also delayed
195 in bradyzoites formed in C2C12 myocytes compared with tachyzoites grown in myoblasts (**Figure 4D**).
196 Bradyzoites cultured in C2C12 myocytes show significantly lower motility in response to A23187 and
197 zaprinast when compared with tachyzoites (**Figure 4E**).

198 To further examine Ca²⁺ signaling in bradyzoites, we harvested tissue cysts containing BAG1-mCherry
199 GCaMP6f bradyzoites from the brains of chronically infected CD-1 mice and investigated their responses ex
200 vivo. Video microscopy of ex vivo tissue cysts showed slow increases in GCaMP6f fluorescence in response
201 to A23187 or zaprinast (**Figure 4F**). The ratio of GCaMP6f fluorescence changes vs time (F/F₀) from
202 bradyzoites within ex vivo cysts demonstrated lower and slower changes, consistent with lower Ca²⁺ levels,
203 compared with extracellular tachyzoites in response to Ca²⁺ agonists (**Figure 4G**). In comparing the response
204 of extracellular, ex vivo tissue cysts (**Figure 4 F,G**) to intracellular cysts formed during infection of C2C12
205 myocytes (**Figure 4 B,C**), it was evident that the extracellular cysts respond somewhat faster, albeit still much
206 slower than tachyzoites. This intermediate level of response was also seen in in vitro differentiated tissue cyst
207 (produced by cultivation in HFF cells at pH 8.2 for 7 days) that were liberated from HFF cells and tested in
208 vitro (**Figure 4-supplement 1**). Next, we measured the percentage of motile and egressed bradyzoites within
209 ex vivo tissue cyst treated with A23187 and zaprinast. Strikingly, no egressed bradyzoites were observed
210 although all the bradyzoites within ex vivo cysts became motile after stimulation (**Figure 4H, Figure 4-video**
211 **1, Figure 4-video 2**). Taken together, these findings indicate that bradyzoites formed spontaneously in muscle
212 myocytes and within ex vivo cysts from chronically infected mice display dampened Ca²⁺ dynamics when
213 treated with Ca²⁺ agonists.

214

215 **Bradyzoites store less Ca²⁺ in ER and acidocalcisome**

216 The cyst wall surrounding bradyzoites may restrict access to Ca²⁺ agonists and hence dampen signals from
217 GCaMP6f in response to Ca²⁺ agonists in the studies described above. To test this possibility, we monitored
218 GCaMP6f fluorescence changes in extracellular bradyzoites vs. tachyzoites of the BAG1-mCherry GCaMP6f
219 strain by live imaging. Bradyzoites were induced by cultivation in HFF cells at pH 8.2 for 7 days and liberated
220 from cysts by trypsin treatment, followed by washing and resuspension for analysis. We also observed slower
221 increases in GCaMP6f fluorescence intensity in bradyzoites (**Figure 5-video 2**) compared with tachyzoites

222 **(Figure 5-video 1)** in response to A23187 **(Figure 5A)**. Quantitative analysis of Ca^{2+} fluorescence changes
223 (F/F_0) after stimulation by A23187 and zaprinast showed slower Ca^{2+} responses in extracellular bradyzoites
224 when compared to tachyzoites **(Figure 5B)**. To confirm that extracellular bradyzoites were viable after
225 liberation from in vitro cultured cysts by trypsin treatment, we utilized SYTOX Red, which is a DNA dye
226 excluded by intact membranes of viable cells. In contrast to bradyzoites that were formaldehyde-fixed as a
227 positive control, extracellular bradyzoites were not stained by SYTOX after the liberation from in vitro cysts
228 **(Figure 5C)**, indicating they were still viable after trypsin treatment.

229 We hypothesized that bradyzoites might have dampened GCaMP6f responses because they fail to release
230 Ca^{2+} from intracellular stores. We tested Ca^{2+} responses of BAG1-mCherry and GCaMP6f -expressing
231 bradyzoites and tachyzoites treated with ionomycin, which releases Ca^{2+} mainly from the ER [50],
232 thapsigargin, which inhibits SERCA-type Ca^{2+} -ATPase causing an increase of cytosolic Ca^{2+} due to
233 uncompensated leakage from the ER [33], and NH_4Cl , an alkalizing reagent that releases Ca^{2+} from acidic
234 stores like acidocalcisomes [35]. Both ionomycin and thapsigargin induced delayed and lower amplitude
235 changes in GCaMP6f fluorescence in bradyzoites vs. tachyzoites as shown by plotting fluorescence intensity
236 fold changes (F/F_0) vs. time **(Figure 5D)**, indicative of lower ER stored Ca^{2+} . In contrast, bradyzoites treated
237 with NH_4Cl showed no meaningful change in GCaMP6f fluorescence, suggesting they lack mobilizable acidic
238 Ca^{2+} **(Figure 5D)**. To rule out the possibility that the Ca^{2+} indicator GCaMP6f is less sensitive in bradyzoites
239 due to some intrinsic defect, we loaded BAG1-mCherry expressing tachyzoite or bradyzoites with the Ca^{2+}
240 sensitive vital dye Fluo-8 AM and used these cells for imaging. Fluo-8 AM labeled bradyzoites displayed
241 dampened Ca^{2+} signaling after stimulation by ionomycin, thapsigargin or NH_4Cl , relative to tachyzoites that
242 responded normally **(Figure 5E)**. Collectively, these findings indicate that bradyzoites are less able to
243 mobilize Ca^{2+} from the ER and acidic stores in response to agonists.

244

245 **Ratiometric sensor reveals reduced basal levels of Ca^{2+} and dynamics in bradyzoites**

246 To more precisely compare Ca^{2+} levels in tachyzoites and bradyzoites, we constructed a ratiometric
247 fluorescence reporter by co-expression of GCaMP6f with blue fluorescent protein mTagBFP2 linked by a P2A
248 split peptide **(Figure 6A, Figure 6 Supplement 1A, Figure 6 Supplement 1B)**. Because both proteins are
249 co-expressed from the same promoter, the mTagBFP2 serves as a control for expression level, as mTagBFP2
250 is non-responsive to Ca^{2+} levels [52]. Live fluorescence microscopy showed simultaneous expression of
251 GCaMP6f and mTagBFP2 in tachyzoites, and additionally mCherry in bradyzoites **(Figure 6B)**. Equal
252 expression of GCaMP6f (His tag) and mTagBFP2, as well as separation of tachyzoites and bradyzoite
253 populations (detected with SAG1 and BAG1 respectively) was validated by western blotting **(Figure 6C)**. To
254 compare Ca^{2+} basal levels, we quantified the fluorescence intensity ratio $F_{\text{GCaMP6f}}/F_{\text{mTagBFP2}}$ of intracellular and
255 extracellular tachyzoites and bradyzoites in EC buffer with or without Ca^{2+} . We observed significant
256 reductions in the fluorescence intensity ratio of both intracellular and extracellular bradyzoites relative to
257 tachyzoites **(Figure 6D)**, indicative of lower resting Ca^{2+} levels in bradyzoites. We next compared Ca^{2+}
258 dynamics of intracellular tachyzoites and bradyzoites in response to Ca^{2+} agonists ionomycin, NH_4Cl and
259 thapsigargin. Changes in the fluorescence of GCaMP6f were much slower and of lower amplitude in
260 bradyzoites relative to tachyzoites **(Figure 6E)**. We also observed lower resting Ca^{2+} and peak levels in

261 extracellular bradyzoites compared to tachyzoites (**Figure 6F**), indicating lower activity or expression of
262 cytoplasmic influx mechanisms like the PM entry or ER release channels. To understand the molecular basis
263 for the reduced stored Ca^{2+} and responses in bradyzoites, we performed real-time PCR to compare mRNA
264 expression levels of TgSERCA [34], which is the drug target of thapsigargin and transfers Ca^{2+} from the
265 cytosol of parasites to ER, TgA1 [36], which plays important roles in the accumulation of Ca^{2+} in the
266 acidocalcisome and other acidic stores, TgTRPPL-2 [53], which is a transient receptor potential (TRP)
267 channel key for Ca^{2+} influx into the cytosol, and other calcium-related proteins, such as TgPMCA1, TgA2 and
268 the $\text{Ca}^{2+}/\text{H}^{+}$ exchanger [54]. We observed significant reduction in the relative expression level of TgSERCA,
269 TgA1, TgPMCA1, TgA2, $\text{Ca}^{2+}/\text{H}^{+}$ exchanger and TgTRPPL-2 in bradyzoites compared to tachyzoites (**Figure**
270 **6G**). Taken together, these findings indicate that bradyzoites have lower levels of stored Ca^{2+} , which is
271 associated with the overall downregulation of Ca^{2+} -related pumps and channels.

272

273 **Calcium signaling plays a critical role in gliding motility of bradyzoites**

274 To test whether dampened Ca^{2+} signaling would still be sufficient to drive gliding motility of bradyzoites, we
275 treated BAG1-mCherry GCaMP6f expressing cysts cultured in vitro with trypsin to liberate bradyzoites
276 (**Figure 7A**). There were no obvious changes in the Ca^{2+} levels nor motility during trypsin treatment and
277 release (**Figure 7B** and **Figure 7-video 1**). When we monitored the motility of released bradyzoites by
278 time-lapse video microscopy, a number of bradyzoites underwent circular gliding (**Figure 7C** and **Figure**
279 **7-video 2**) in patterns that were highly reminiscent of tachyzoite motility. Similar to previous descriptions of
280 oscillating Ca^{2+} patterns in gliding tachyzoites [39], we observed fluctuations of GCaMP6f fluorescence
281 intensities in single extracellular bradyzoites with gliding motility (**Figure 7D**).

282 To further characterize the role of Ca^{2+} signaling in bradyzoites motility, we treated cells with the Ca^{2+}
283 chelator BAPTA-AM, the PKG inhibitor compound 1, and the CDPK1 inhibitor 3-MB-PP1 to block Ca^{2+}
284 signaling in bradyzoites. All these inhibitors significantly impaired gliding motility of tachyzoites and
285 bradyzoites (**Figure 7E** and **Figure 7F**), confirming a key role of Ca^{2+} signaling in parasite motility.
286 Bradyzoites displayed shorter gliding distance compared with tachyzoites as determined by measurements of
287 trail lengths detected with SAG1 (tachyzoite) or SRS9 (bradyzoites) (**Figure 7F**). In summary, despite having
288 dampened Ca^{2+} stores and reduced responses to agonist when intracellular, extracellular bradyzoites require
289 calcium signaling to activate gliding motility.

290

291 **Accumulation of calcium stores and ATP synergistically activates gliding motility by bradyzoites**

292 Following reactivation of tissue cysts, we hypothesize that bradyzoites must replenish their Ca^{2+} and energy
293 stores to meet the demands of cell to cell transmission. To test this idea, we released bradyzoites using trypsin
294 treatment and then treated extracellular bradyzoites with EC buffer with or without Ca^{2+} (1.8 mM) and with or
295 without glucose (5.6 mM) for different times and stimulated the calcium responses using ionomycin.
296 Quantitative analysis of Ca^{2+} fluorescence changes (F/F_0) showed that bradyzoites recovered substantial stored
297 Ca^{2+} in the presence of exogenous Ca^{2+} and glucose for 1 hr compared to 10 min (**Figure 8A** and **8B**). A more

298 modest recovery was observed in the presence of Ca^{2+} but absence of glucose (**Figure 8B**). Next, we
299 investigated the effect of exogenous Ca^{2+} and glucose on gliding motility by bradyzoites. We used time-lapse
300 video microscopy to determine the percentage of extracellular bradyzoites undergoing twirling, circular and
301 helical motility after incubation in EC buffer $\pm \text{Ca}^{2+}$ and glucose for 10 min vs 1 hr. Quantitative analysis
302 showed that bradyzoites underwent all forms of gliding motility and substantially recovered gliding motility
303 after incubation with EC buffer containing both Ca^{2+} and glucose for 1 hr, while very few bradyzoites were
304 able to glide following incubation with exogenous Ca^{2+} or glucose alone (**Figure 8C**).

305 We reasoned that exogenous glucose could be utilized by parasites to produce ATP via glycolysis or
306 oxidative phosphorylation to maintain a variety of cellular functions. To investigate the ATP source for
307 supporting gliding motility, we treated exogenous bradyzoites in EC buffer containing Ca^{2+} (1.8 mM) with
308 glucose to support glycolysis vs. the glucose analogue 2-deoxy-D-glucose (2-DOG) to block glycolysis
309 (**Figure 8D**). Alternatively, similar preparations of bradyzoites were incubated with glutamine to provide
310 substrates for the tricarboxylic acid (TCA) cycle or the ATP synthase inhibitor oligomycin A to inhibit
311 oxidative phosphorylation (**Figure 8D**). Quantitative analysis of percentage of gliding motility showed either
312 glucose or glutamine significantly increased gliding motility by bradyzoites (**Figure 8E**), indicating that either
313 carbon source can be used to produce ATP for maintaining gliding motility. Either 2-DOG or oligomycin A
314 blocked gliding motility by bradyzoites even in the presence of exogenous glucose or glutamine (**Figure 8E**),
315 demonstrating that both oxidative phosphorylation and glycolysis are ATP sources for driving gliding motility
316 by bradyzoites.

317 To further investigate the energy status of bradyzoites, we utilized reversed-phase high-performance
318 liquid chromatography (RP-HPLC) to measure the adenosine triphosphate (ATP), adenosine diphosphate
319 (ADP) and adenosine monophosphate (AMP) levels in bradyzoites treated with EC buffer containing both
320 Ca^{2+} (1.8 mM) and glucose (5.6 mM) for different time (**Figure 8-supplement 1A, 1B and 1C**). We observed
321 that after the incubation in EC buffer for 1 hr, bradyzoites had significantly higher ATP, ADP and AMP levels
322 (**Figure 8F**), demonstrating enhanced ATP production during incubation. The ATP/ADP ratio and energy
323 charge have been widely used to evaluate cellular energy status, which controls the free-energy change for
324 ATP hydrolysis for different cellular functions [55]. Bradyzoites incubated with EC buffer for 1 hr displayed
325 significantly increased ATP/ADP ratio and energy charge (**Figure 8G and 8H**), indicating bradyzoites rapidly
326 recover their energy status following incubation with glucose. Collectively, exogenous Ca^{2+} and glucose
327 altogether activate bradyzoite gliding motility via restoration of ATP levels and Ca^{2+} stores.

328 Discussion

329 Calcium signaling plays important roles in the control of microneme secretion, gliding motility, and egress
330 of apicomplexan parasites and these pathways have been extensively characterized in the tachyzoite stage of *T.*
331 *gondii* [8,30], although not widely explored in other motile life cycle stages. Here we compared the responses
332 of *T. gondii* tachyzoites and bradyzoites to Ca^{2+} ionophores and agonists that cause release of Ca^{2+} from
333 intracellular stores and found that Ca^{2+} responses, microneme secretion, and egress by bradyzoites were all
334 highly attenuated. Dampened Ca^{2+} responses were evident in the responses of in vitro cysts differentiated

335 under stress conditions, naturally occurring cysts formed in muscle cells, and tissue cysts purified from brains
336 of chronically infected mice and tested *ex vivo*. Reduced responses were not simply a consequence of the
337 intracellular environment, as similar dampened Ca^{2+} signals and microneme secretion were observed in single,
338 extracellular bradyzoites. Ratiometric Ca^{2+} imaging revealed lower resting Ca^{2+} levels and reduced ER and
339 acidic stored Ca^{2+} in bradyzoites, which is likely a reflection of down-regulation of Ca^{2+} -ATPases involved in
340 maintaining these stores replenished. Tissue cysts are characterized by a thick wall comprised of proteins and
341 carbohydrates which may collectively impede signals and/or restrict egress mechanically. However, when
342 cysts were digested by trypsin to release bradyzoites, they exhibited Ca^{2+} -dependent gliding motility that was
343 enhanced by incubation in extracellular Ca^{2+} in combination with glucose, demonstrating that they express a
344 conserved mechanism for Ca^{2+} mediated motility, albeit dampened by reduced stored Ca^{2+} and diminished
345 energy levels. The dampened Ca^{2+} signaling responses of bradyzoites reflect adaptations that are well suited to
346 the long-term intracellular lifestyle of these chronic stages. As well, bradyzoites retain the potential to rapidly
347 become motile once provided with sources of energy and calcium, demonstrating remarkable physiological
348 flexibility that favors transmission.

349 Egress is a crucial step in the lytic cycle of apicomplexan parasites and this response requires the
350 sequential steps of increase in cytoplasmic Ca^{2+} , secretion of micronemes, PV rupture, and activation of
351 motility [56,57]. Our studies demonstrate that bradyzoites show minimal egress from *in vitro* differentiated
352 cysts in response to agonists that normally trigger this response in tachyzoites (i.e. Ca^{2+} ionophores and
353 zaprinast). We also demonstrate that bradyzoites are refractory to stimulation of microneme secretion using
354 either an intracellular reporter monitoring the release of PLP1 based on the dispersion of FNR-mCherry from
355 the cyst matrix, or a MIC2-GLuc reporter detecting secretion from extracellular bradyzoites. To explore the
356 basis for these differences, we utilized a dual fluorescent reporter GCaMP6f BAG1-mCherry to monitor
357 changes of cytosolic Ca^{2+} levels in bradyzoites. Calcium signaling was significantly dampened in bradyzoites
358 as reflected in delayed Ca^{2+} spikes and lower magnitude of cytosolic Ca^{2+} increases in response to Ca^{2+}
359 agonists. Reduced Ca^{2+} responses were also confirmed using bradyzoites naturally formed in C2C12 skeletal
360 muscle cells and *ex vivo* cysts isolated from chronically infected mice, indicating that the dampened responses
361 are not simply a consequence of alkaline pH stress during bradyzoites development *in vitro*. Additionally, we
362 observed similar dampened responses from extracellular bradyzoites, indicating that decreased responses are
363 not simply due to reduced permeability of intact cysts to agonists. To confirm these results, we also utilized
364 Fluo-8/AM to monitor intracellular Ca^{2+} stores of bradyzoites and observed similar dampened responses.
365 Finally, since Ca^{2+} -dependent fluorescence responses by GCaMP6f or Fluo-8 are only relative and subject to
366 differences in protein or probe levels, we developed a ratiometric calcium reporter that contains GCaMP6f
367 fused with self-cleavage tag P2A linked mTagBFP2 under the control of the same promoter. Ratiometric
368 measurements of the GCaMP6f signal compared to the Ca^{2+} insensitive indicator mTagBFP2, determined that
369 bradyzoites have lower resting Ca^{2+} levels and quantitatively decreased Ca^{2+} responses relative to tachyzoites
370 in response to Ca^{2+} agonists. Collectively, these findings conclusively show that bradyzoites have reduced Ca^{2+}
371 responses whether developed *in vitro* or *in vivo* and using a variety of independent methods to assess both
372 Ca^{2+} levels and physiological responses.

373 Based on the above findings, it seems likely that bradyzoites possess different mechanisms to control Ca^{2+}

374 homeostasis, including differences in expression of Ca²⁺ channels and Ca²⁺ pumps relative to tachyzoites.
375 These differences would impact Ca²⁺ storage pools, affecting cytosolic Ca²⁺ and signaling. For example, our
376 findings indicate that bradyzoites show reduced responses to ionomycin and thapsigargin, which release Ca²⁺
377 from the ER, and in response to NH₄Cl, which releases Ca²⁺ from acidocalcisomes and likely other acidic
378 stores [35,58]. Consistent with these dampened responses, bradyzoites showed significantly reduced
379 expression of the Ca²⁺-ATPases TgSERCA [34] and TgA1 [36], which are involved in transporting cytosolic
380 Ca²⁺ into the ER and acidocalcisome, respectively. They also showed reduced expression of TgA2, the Ca²⁺/H⁺
381 exchanger and the recently described TRPPL-2 [53], which is a transient receptor potential (TRP) channel key
382 for cytosolic Ca²⁺ influx through the plasma and ER membranes. The reduced expression of these genes is
383 also supported by prior data on stage-specific transcriptional differences (<http://Toxodb.org>). Additionally, it is
384 possible that the reduced levels of Ca²⁺ in bradyzoites reflect limitations on the availability of Ca²⁺ from the
385 host cell, since prior studies have shown that tachyzoites acquire their intracellular Ca²⁺ from this source [37].
386 Further studies will be needed to decipher the contribution of these various mechanism to altered calcium
387 homeostasis and signaling in bradyzoites.

388 Bradyzoites are surrounded by a cyst wall that is comprised of an outer thin compact layer and an inner
389 sponge-like layer that faces the cyst matrix [59]. The cyst wall is enriched in dense granule proteins [60],
390 stage-specific glycoproteins such as CST1 [61,62], and partially characterized carbohydrates [63]. This
391 architecture may create a barrier to egress since bradyzoites were able to activate motility but not to efficiently
392 emerge from intact cysts. We utilized trypsin to digest the cyst wall, mimicking the cyst rupture observed in
393 chronically infected mice or following oral ingestion and exposure to pepsin [43,64]. Notably, proteolytic
394 release did not result in immediate changes in Ca²⁺ nor motility in the parasite, suggesting that cyst wall
395 degradation does not trigger a process akin to egress in tachyzoites. Rather, when artificially released in this
396 manner, a subset of bradyzoites spontaneously underwent gliding motility associated with Ca²⁺ oscillations
397 that were similar to those previously described for tachyzoites [39]. When incubated with extracellular Ca²⁺,
398 the percentage of motile bradyzoites increased dramatically, suggesting that Ca²⁺ entry stimulates motility,
399 similar to tachyzoites [14,41]. Unlike a previous report showing that tachyzoites contain sufficient calcium
400 stores and energy levels to be independent of external carbon sources during the first hr after liberation [65],
401 we observed that bradyzoites require an external source of carbon to regain Ca²⁺ stores and ATP levels.
402 Similar to previous findings that *T. gondii* tachyzoites can support motility either from glucose through
403 glycolysis or from glutamine that feeds into the TCA cycle [66,67], we observed that either carbon source was
404 capable of synergizing with Ca²⁺ to restore bradyzoite motility, although inhibitor studies indicate that
405 oxidative phosphorylation is required to restore optimal energy levels. Consistent with this prediction, we
406 observed that bradyzoites have intrinsically low ATP/ADP ratios but that they recovered substantially when
407 incubated extracellularly for 1 hr in Ca²⁺ and glucose. Hence, reduced expression of Ca²⁺ channels that allow

408 influx into the cytosol and reduced expression of Ca^{2+} pumps that fill intracellular stores would result in a
409 general reduction of stored Ca^{2+} . Reduced ER Ca^{2+} could impact mitochondrial Ca^{2+} , since it has been
410 shown in mammalian cells that Ca^{2+} can be transferred directly (through membrane contact sites) from the ER
411 to the mitochondria [68,69], which is essential for oxidative phosphorylation and ATP production. Ultimately,
412 reduced ER Ca^{2+} may be responsible for altering energy metabolism and inducing the quiescent state in *T.*
413 *gondii* bradyzoites. Collectively, these findings indicate that bradyzoites are characterized by both low
414 calcium stores and low ATP levels, but that they respond rapidly to changes in the extracellular environment to
415 restore both energy levels and Ca^{2+} signaling systems needed for motility. Stimulation of Ca^{2+} signaling is also
416 important in breaking dormancy [70] and pollen germination in plants [71], and initiation of the cell cycle in
417 animal cells [72], demonstrating the important role played by Ca^{2+} signaling in reactivation.

418 Reduced Ca^{2+} storage, dampened Ca^{2+} signaling, and a lower energy state may reflect the long-term
419 sessile nature of the intracellular cyst, which prolong chronic infection. The mechanisms inducing cyst wall
420 turnover in vivo are unclear, although host cell macrophages may contribute to this process as they secrete
421 chitinase that can lyse cysts in vitro [73]. Additionally, cyst wall turnover may be controlled by release of
422 parasite hydrolases as suggested by the presence of GRA56, which is predicted to belong to the melibiase
423 family of polysaccharide degrading enzymes, on the cyst wall [74]. Our in vitro studies suggest that once the
424 cyst wall is ruptured, bradyzoites respond to higher levels of Ca^{2+} and glucose in the extracellular environment
425 to regain motility needed for subsequent cell invasion. Emergence of bradyzoites from tissue cysts that rupture
426 in muscle or brain, or in tissue following oral ingestion, are likely to provide an environment to recharge
427 bradyzoites. Consistent with this idea, previous in vitro studies have shown that similar motile bradyzoites
428 released from ruptured cysts have the ability to re-invade new host cells, establishing new cysts without an
429 intermediate growth stage as tachyzoites [75]. Hence, the rapid metabolic recovery of otherwise quiescent
430 bradyzoites may be important for the maintenance of chronic infection within a single host and to assure
431 robust cellular invasion upon transmission to the next host.

432

433 **Materials and Methods**

434 **Cell culture**

435 *Toxoplasma gondii* tachyzoites were passaged in confluent monolayers of human foreskin fibroblasts (HFFs)
436 obtained from the Boothroyd laboratory at Stanford University. The ME49 $\Delta\text{hxgprt}::\text{Fluc}$ type II strain of *T.*
437 *gondii* [76] was used as a parental strain for genetic modification. Tachyzoites were cultured in Dulbecco's
438 modified Eagle's medium (DMEM; Life Technologies) pH 7.4, supplemented with 10% fetal bovine serum
439 (FBS), penicillin, and streptomycin (Life Technologies) at 37°C in 5% CO_2 . For in vitro induction of
440 bradyzoites, parasites were cultured in alkaline medium in ambient CO_2 as described previously [77]. In brief,
441 infected HFF monolayers were switched to RPMI 1640 medium (MP Biomedicals) buffered to pH 8.2 with
442 HEPES and supplemented with 5% FBS and cultured at 37°C in ambient CO_2 , during which time the alkaline
443 medium was changed every 2 days. For spontaneous induction of bradyzoites, C2C12 muscle myoblast cells

444 (ATCC[®] CRL-1772[™]) were maintained in DMEM supplemented with 20% FBS. C2C12 myoblast
445 differentiation and myotube formation were induced in DMEM containing 2% horse serum (Biochrom) by
446 cultivation at 37°C in 5% CO₂ for 5 days. Tachyzoites were inoculated into the differentiated muscle cells and
447 cultured for another 7 days to induce bradyzoite formation, during which time the induction medium was
448 changed every 2 days. For harvesting bradyzoites, infected monolayers were scraped into intracellular (IC)
449 buffer (142 mM KCl, 5 mM NaCl, 1 mM MgCl₂, 5.6 mM D-glucose, 2 mM EGTA, 25 mM HEPES, pH 7.4)
450 and released from cells by serially passing through 18g, 20g and 25g needles, followed by centrifugation
451 (150g, 4°C) for 10 min. The pellet containing cysts was resuspended in IC buffer. Bradyzoites were liberated
452 from cysts by digestion with 0.25 mg/ml trypsin at room temperature for 5 min, followed by centrifugation
453 (150g, 4°C) for 10 min. The supernatant containing liberated bradyzoites was further centrifuged (400g, 4°C)
454 for 10 min. The pellet containing purified bradyzoites was resuspended in extracellular (EC) buffer (5 mM
455 KCl, 142 mM NaCl, 1 mM MgCl₂, 5.6 mM D-glucose, 25 mM HEPES, pH 7.4) with (1.8 mM Ca²⁺) or
456 without CaCl₂, as indicated for different assays and in the legends.

457 **Reagents and antibodies**

458 A23187, zaprinast, ionomycin, thapsigargin, NH₄Cl, Fluorescein isothiocyanate-conjugated *Dolichos biflorus*
459 agglutinin (DBA), and BAPTA-AM were obtained from Sigma. Fluo-8 AM was obtained from Abcam.
460 SYTOX[™] Red Dead Cell Stain was obtained from Thermal Fisher. The compounds 3-MB-PP1 [51] and
461 Compound 1 [42] were obtained as described previously. Trypsin and L-glutamine were purchased from MP
462 Biomedicals. Adenosine 5'-triphosphate (ATP) disodium salt, adenosine 5' -diphosphate (ADP) sodium salt,
463 adenosine 5' -monophosphate (AMP) disodium salt, oligomycin A and 2-deoxy-D-glucose were purchased
464 from Sigma. Primary antibodies include mouse mAb DG52 anti-SAG1 (provided by John Boothroyd), mouse
465 mAb 6D10 anti-MIC2 [78], rabbit anti-GRA7 [79], mouse mAb 8.25.8 anti-BAG1 (obtained from Louis
466 Wiess), rabbit anti-BAG1 (obtained from Louis Wiess), mouse anti-c-myc (mAb 9E10, Life Technologies),
467 mouse anti-acetylated Tubulin (mAb 6-11B-1, Sigma), rat anti-mCherry (mAb 16D7, Life Technologies),
468 rabbit-anti SRS9 (obtained from John Boothroyd), rabbit anti-tRFP (Axxora), mouse anti-6XHis (mAbHIS.H8,
469 Life Technologies). Secondary antibodies for immunofluorescence assays include goat anti-mouse IgG
470 conjugated to Alexa Fluor-488, goat anti-rabbit IgG conjugated to Alexa Fluor-488, anti-mouse IgG
471 conjugated to Alexa Fluor-568, goat anti-rat IgG conjugated to Alexa Fluor-568, goat anti-mouse IgG
472 conjugated to Alexa Fluor-594 (Life Technologies). For Western blotting, secondary antibodies consisted of
473 goat anti-mouse IgG, goat anti-rabbit IgG, or goat anti-rat IgG conjugated to LiCor C800 or C680 IR-dyes and
474 detected with an Odyssey Infrared Imaging System (LI-COR Biotechnology).

475 **Generation of stable transgenic parasite lines**

476 *Dual calcium and bradyzoite reporter strain: BAG1-mCherry GCaMP6f*

477 A dual reporter stain designed to detect bradyzoite conversion and calcium fluctuation was generated in the
478 ME49 $\Delta h x g p r t :: F l u c$ strain [76]. We generated a plasmid named pNJ-26 that contains mCherry driven by the
479 BAG1 promoter, the genetically encoded calcium indicator GCaMP6f under the control of Tubulin1 promoter,
480 and selection marker cassette SAG1 promoter driving CAT. ME49 $\Delta h x g p r t :: F l u c$ tachyzoites were transfected
481 with 20 μ g pNJ-26 plasmid and selected with 20 μ M chloramphenicol. Clones containing randomly integrated
482 transgenes were confirmed by diagnostic PCR and by IFA staining. Primers are shown in Supplementary table

483 1.

484 *Bradyzoite reporter strain: BAG1-EGFP and BAG1-mCherry*

485 The BAG1 promoter and the mCherry open reading frame (ORF) were independently PCR amplified from
486 pNJ-26 and the EGFP ORF was amplified from pSAG1:CAS9-U6:sgUPRT respectively. The BAG1 promoter
487 fragment and EGFP ORF or mCherry (ORF) were cloned by NEBuilder HiFi DNA Assembly Cloning Kit
488 (NEB, E5520S) into the vector backbone that was produced by double enzymatic digestion of
489 pTUB1:YFP-mAID-3HA, DHFR-TS:HXGPRT using KpnI and NdeI. ME49 *Δhxgprt::Fluc* tachyzoites were
490 transfected with 20 μg pBAG1:EGFP, DHFR-TS:HXGPRT or pBAG1:mCherry, DHFR-TS:HXGPRT and
491 selected with mycophenolic acid (MPA) (25 μg/ml) and 6-xanthine (6Xa) (50 μg/ml). Single cell clones
492 containing randomly integrated transgenes were confirmed by diagnostic PCR and by IFA staining. Primers
493 are shown in Supplementary table 1.

494 *MIC2 secretion reporter BAG1-mCherry MIC2-GLuc*

495 The bradyzoite reporter line BAG1-mCherry was transfected with 20 μg of the previously described
496 pMIC2:GLuc-myc, DHFR-TS plasmid [42] and selected with 3 μM pyrimethamine (PYR). Single cell clones
497 containing randomly integrated transgenes were confirmed by diagnostic PCR and by IFA staining.

498 *FNR-mCherry leakage reporter BAG1-EGFP FNR-mCherry*

499 The bradyzoite reporter line BAG1-EGFP was transfected with 20 μg pTUB1:FNR-mCherry, CAT (provided
500 by the Carruthers lab) and selected with 20 μM chloramphenicol. Single cell clones containing randomly
501 integrated transgenes were confirmed by diagnostic PCR and by IFA staining.

502 *Ratiometric reporter BAG1-mCherry GCaMP6f-P2A-mTagBFP2*

503 The ratiometric reporter strain was generated using targeted insertion with CRISPR/Cas9 using previously
504 described methods [80] to add the blue fluorescent protein (BFP) downstream of the GCaMP6f protein in the
505 strain BAG1-mCherry GCaMP6f. In brief, a single guide RNA (sgRNA) targeting the DHFR 3'UTR
506 following the GCaMP6f coding sequence was generated in the plasmid pSAG1:CAS9-U6:sgUPRT [81]. The
507 P2A-mTagBFP2 tagging plasmid was constructed by cloning a synthetic sequence containing a split peptide
508 (P2A) together with the blue fluorescent reporter mTagBFP2 (P2A-mTagBFP2) into the
509 pTUB1:YFP-mAID-3HA, DHFR-TS:HXGPRT backbone by NEBuilder HiFi DNA Assembly Cloning Kit
510 (NEB, E5520S) after double enzymatic digestion of KpnI and NdeI. Following this step, the SAG1 3'UTR
511 was amplified from pNJ-26 and cloned into the tagging plasmid to replace DHFR 3'UTR by Gibson assembly
512 (NEB, E5520S). BAG1-mCherry GCaMP6f reporter tachyzoites were co-transfected with 10 μg of
513 pSAG1::CAS9-U6::sgDHFR 3'UTR and 2 μg of PCR amplified P2A-mTagBFP2-HXGPRT flanked with 40
514 bp homology regions, as described previously [26]. Stable transfectants were selected with 25 μg/ml MPA and
515 50 μg/ml 6Xa. Single cell clones containing targeted integrated transgenes were confirmed by diagnostic PCR
516 and by IFA staining. Primers are shown in Supplementary Table S1.

517 **Time-lapse imaging of fluorescent reporter strains**

518 For time-lapse microscopy, extracellular parasites were added to glass-bottom culture dishes (MatTek), or
519 intracellular parasites were grown in host cells attached glass-bottom culture dishes. Alternating phase and
520 fluorescent images (at different intervals specified in the legends) were collected on a Zeiss AxioObserver Z1
521 (Carl Zeiss, Inc.) equipped with an ORCA-ER digital camera (Hamamatsu Photonics) and a 20x EC

522 Plan-Neofluar objective (N.A. 0.50), 37°C heating unit, and LED illumination for blue, green, red and far-red
523 wavelengths. Spinning disk images were acquired with a 100x oil Plan-Apochromat (N.A. 1.46) objective
524 using illumination from 488 nm and 561 nm solid state lasers (Zeiss) and Evolve 512 Delta EMCCD cameras
525 (Photometrics) attached to the same Zeiss AxioObserver Z1 microscope. Images were acquired and analyzed
526 using Zen software 2.6 blue edition (Zeiss). Fluorescent intensity changes (F/F_0) vs. time were plotted with
527 GraphPad Prism version 6 (GraphPad Software, Inc.).

528 **Indirect immunofluorescence assay (IFA)**

529 Parasites grown in HFF monolayers on glass coverslips were fixed in 4% (v/v) formaldehyde in PBS for 10
530 min, and permeabilized by 0.25% (v/v) Triton X-100 in PBS for 20 min, and blocked in 3% bovine serum
531 albumin (BSA) in PBS. Monolayers were incubated with different primary antibodies and visualized with
532 secondary antibodies conjugated to Alexa Fluors. Coverslips were sealed onto slides using ProLong™ Gold
533 Antifade containing DAPI (Thermo Fisher Scientific). Images were captured using a 63x oil Plan-Apochromat
534 lens (N.A. 1.4) on an Axioskop2 MOT Plus Wide Field Fluorescence Microscope (Carl Zeiss, Inc). Scale bars
535 and linear adjustments were made to images using Axiovision LE64 software (Carl Zeiss, Inc.).

536 **Western Blotting**

537 Samples were prepared in 5X Laemmli buffer containing 100 mM dithiothreitol, boiled for 5 min, separated
538 on polyacrylamide gels by SDS-PAGE, and transferred to nitrocellulose membrane. Membranes were blocked
539 with 5% nonfat milk, probed with primary antibodies diluted in blocking buffer. Membranes were washed
540 with PBS + 0.1% Tween 20, then incubated with goat IR dye-conjugated secondary antibodies (LI-COR
541 Biosciences) in blocking buffer. Membranes were washed several times before scanning on a LiCor Odyssey
542 imaging system (LI-COR Biosciences).

543 **Fluo-8 AM calcium monitoring**

544 Freshly harvested parasites were loaded with 500 nM Fluo-8 AM for 10 min at room temperature, followed by
545 centrifugation at 400 g for 5 min and washing in EC buffer without Ca^{2+} . Parasites were resuspended in EC
546 buffer without Ca^{2+} and added directly to glass-bottom culture dishes. After addition of agonists, time-lapse
547 images were recorded and analyzed as described above.

548 **Egress assay**

549 Infected cells were treated with 2 μ M A23187 or 500 μ M zaprinast for 15 min at 37°C. Following incubation,
550 samples were stained by IFA using antibodies against SAG1 (mouse), GRA7 (rabbit), FITC-conjugated DBA
551 or BAG1 (rabbit) and followed by secondary antibodies conjugated to Alexa Fluors. Samples were examined
552 by fluorescence microscopy and the percentages of egressed or released parasites per vacuole or cyst were
553 determined at least for 20 vacuoles or cysts per experiment. The maximum egress distance of parasites from
554 vacuole or cysts were measured from scanned tiff images in imageJ.

555 **Flow cytometry**

556 ME49 BAG1-mCherry MIC2-GLuc reporter bradyzoites were induced for 7 days at pH 8.2, harvested in IC
557 buffer as described above, and passed through 5 μ m polycarbonate membrane filter. ME49 Δ *hxgprt::Fluc*
558 tachyzoites, cultured and harvested as indicated above, were used for gating. Approximately 1×10^6 parasites
559 from each sample (ME49 BAG1-mCherry MIC2-GLuc reporter tachyzoites and ME49 BAG1-mCherry
560 MIC2-GLuc reporter bradyzoites) were sorted on Sony SH800S Cell Sorter directly into 500 μ l IC buffer

561 followed by centrifugation. Flow cytometry data were processed using FlowJo version 10 (FLOWJO, LLC).

562 **Collection of excretory-secretory antigens (ESA) and Gaussia Luciferase Assay**

563 FACS sorted MIC2-GLuc reporter tachyzoites and bradyzoites were suspended with EC buffer and incubated
564 with different agonists at 37°C for 10 min. ESA was collected by centrifugation and mixed with Pierce™
565 *Gaussia* Luciferase Glow Assay Kit reagent (Thermo Scientific™) and luminescence was detected using a
566 Cytation 3 Cell Imaging Multimode Imager (BioTek Instruments, Inc.). Buffer control values were subtracted
567 from their corresponding sample values to correct for background.

568 **Real-time PCR**

569 RNA was extracted from ME49 *Δhxprrt::Fluc* tachyzoites and bradyzoites induced for 7 days at pH 8.2 using
570 RNeasy Mini Kit (Qiagen) combined with QIAshredder (Qiagen) followed by DNA Removal using
571 DNA-free™ DNA Removal Kit (Thermo Fisher) and subsequent reverse transcription using High-Capacity
572 cDNA Reverse Transcription Kit (Thermo Fisher). Quantitative real-time PCR was performed on Applied
573 Biosystems QuantStudio 3 Real-Time PCR System (Thermo Fisher) using SYBR® Green JumpStart™ Taq
574 ReadyMix™ (Sigma) with primers shown in Supplementary table 1. Mean fold changes from two
575 independent experiments were calculated from $\Delta\Delta$ Ct values using actin1 transcript as housekeeping gene, as
576 described previously [82].

577 **Gliding trail assay**

578 Coverslips were pre-coated by incubation in 50% fetal bovine serum diluted in PBS for 1 h at 37°C followed
579 by rinsing in PBS. Freshly harvested tachyzoites or bradyzoites were resuspended in EC buffer, treated with
580 DMSO (0.1%, v/v), or inhibitors (in 0.1% DMSO, v/v) and then added to pre-coated glass coverslips and
581 incubated at 37°C for 15 min. Coverslips were fixed in 2.5% formalin in PBS for 10 min and the surface
582 proteins were detected by IFA as above described using anti-SAG1 and anti-SRS9 antibodies as stage-specific
583 markers for tachyzoites and bradyzoites, respectively. Gliding trails were captured by IFA microscopy as
584 described above and the frequency of trails measured from tiff images using ImageJ.

585 **Gliding motility assay based on time-lapse video microscopy**

586 BAG1-mCherry parasites were induced to form bradyzoites by culture at pH 8.2 in RPMI 1640 medium under
587 ambient air (low CO₂) for 7 days followed by scraping into IC buffer (without glucose) and repeated passage
588 through a 23g needle. Intact, but extracellular cysts, were pellet by centrifugation at 150 g for 10 min and
589 resuspended in IC buffer without glucose. During purification, all procedures were performed at 16°C.
590 MatTek 25 mm dishes glass bottom dishes (coverslip dishes) were pre-coated with 2 ml 50% FBS at 4°C
591 overnight and rinsed twice using PBS prior to use. Purified cysts were added to the pre-coated coverslip dishes
592 in IC buffer containing 0.25mg/ml trypsin and incubated for 10 min at 16°C. The medium was removed and 2
593 ml EC buffer \pm 1.8 mM Ca²⁺ and/or \pm 5.6 mM glucose was added and incubated for 10 min or 1 hr at 16°C.
594 Prior to imaging, the coverslip dishes were heated to 37 °C using a Heating Unit XL S (Zeiss) attached to the
595 Zeiss AxioObserver Z1 (Carl Zeiss, Inc.). Images were collected under bright field illumination using a 40x
596 C-Apochromat water immersion objective (N.A. 1.20), and ORCA-ER digital camera (Hamamatsu Photonics
597 at 1 sec intervals for 5 min per field. The percentage of BAG1-mCherry positive bradyzoites displaying
598 different types of gliding motility was calculate from 6 movies per sample. Images were imported into NIH
599 ImageJ with a Cell Counter plug-in for quantification of the types of motility based on visual inspection.

600 **High-performance liquid chromatography UV (HPLC-UV) analysis of ATP, ADP and AMP levels in**
601 **bradyzoites** BAG1-mCherry parasites were induced to form bradyzoites by culture at pH 8.2 in RPMI 1640
602 medium under ambient air (low CO₂) for 7 days followed by scraping into ice-cold PBS containing 0.05%
603 BSA. Cysts were released from host cells by repeated passage through a 23 g needle and collected by
604 centrifugation at 150 g for 10 min. To purify bradyzoites, cysts were resuspended in 1 ml EC buffer without
605 calcium or glucose but containing 10 µl biotinylated DBA (Vector laboratories) and 100 ul Pierce Streptavidin
606 Magnetic Beads (Thermo Fisher) and incubated for 1 hr at 4°C. The beads and absorbed cysts were collected
607 using a magnetic stand and resuspended in 1 ml EC buffer without calcium or glucose but containing 0.25
608 mg/ml trypsin and incubated for 10 min at 4°C. The supernatant containing released parasites was separated
609 from the beads and retained. To remove any residual tachyzoites in the supernatant, 5 ul of mAb DG52
610 pre-coupled to 100 µl Dynabeads™ Protein G (Thermo Fisher) was added to the supernatant and incubated
611 for 1 hr at 4°C. The supernatant was separated from the beads, bradyzoites centrifuged at 600 g, 4°C for 10
612 min, and resuspended in 1 ml EC buffer containing 1.8 mM Ca²⁺ and 5.6 mM glucose for 10 min or 1 hr at
613 room temperature. Following incubation, the bradyzoites were pelleted at 600 g, 4°C for 10 mi and stored at
614 -80°C until analysis.

615 A previously described method for extraction of ATP, ADP and AMP [83] was adapted for use here. In
616 brief, 95 µl of extraction buffer (0.3 M perchloric acid (HClO₄), 1 mM ethylenediaminetetraacetic acid
617 disodium salt (Na₂EDTA), pH 8.0) was used to resuspend cell pellets and incubated for 5 min at room
618 temperature. Extraction was stopped by addition of 17 µl of neutralization buffer (2 M potassium hydroxide)
619 to the samples followed by mixing. Samples were centrifuged at 14,000 g for 10 min at 4°C and the
620 supernatant was transferred to a new tube for HPLC analysis. Analysis was performed using an HPLC system
621 consisting of a SPD-20A UV/VIS detector (Shimadzu) equipped with SIL-20A autosampler (Shimadzu), with
622 a Luna Omega Polar C18 column (4.6 mm internal diameter × 150 mm length, 3 µm particle size, 100 Å pore
623 size), and LC-20AD pump (Shimadzu). The protocol was set up as isocratic separation using a mobile phase
624 containing 0.1 M ammonium dihydrogen phosphate (NH₄H₂PO₄, Sigma), pH 6.0, containing 1% methanol
625 with a flow rate of 0.8 ml/min. Injection volume was 30 µl and peak detection was monitored at 254 nm. A
626 series of standards containing ATP, ADP and AMP with different concentrations were used to establish
627 retention times and standard calibration curves by calculating peak area. Samples from two independent
628 biological replicates were analyzed using three technical replicates. The retention time and peak areas were
629 used to calculate the corresponding concentration of each nucleotide from each sample according to the
630 standard curve.

631 **Mouse infections and ex vivo cyst collection**

632 Mice were housed in an Association for Assessment and Accreditation of Laboratory Animal Care
633 International-approved facility at Washington University School of Medicine. All animal studies were
634 conducted in accordance with the U.S. Public Health Service Policy on Humane Care and Use of Laboratory
635 Animals, and protocols were approved by the Institutional Animal Care and Use Committee at the School of
636 Medicine, Washington University in St. Louis.

637 Eight-week old female CD-1 mice (Charles River) were infected with 200 ME49 BAG1-mCherry GCaMP6f

638 tachyzoites by intraperitoneal injection. After 30 days of infection, animals were sacrificed, the brain removed
639 and homogenized and the number of brain cyst was determined by DBA staining and microscopy as
640 previously described [77]. Eight-week old female CD-1 mice (Charles River) were infected with 5 cysts from
641 the brain homogenate by oral gavage. Following a 30-day period these mice were euthanized, and brain
642 homogenate was collected and added to glass bottom dishes for live imaging of tissue cysts.

643 **Statistical Analyses**

644 Statistical analyses were performed in Prism (GraphPad). Data that passed normally distribution were
645 analyzed by one-way ANOVA or Student's t tests, while data that were not normally distributed, or contain too
646 few samples to validate the distribution, were analyzed by Mann Whitney or Kruskal-Wallis non-parametric
647 tests. *, $P < 0.05$, **, $P < 0.01$, ***, $P < 0.001$.

648

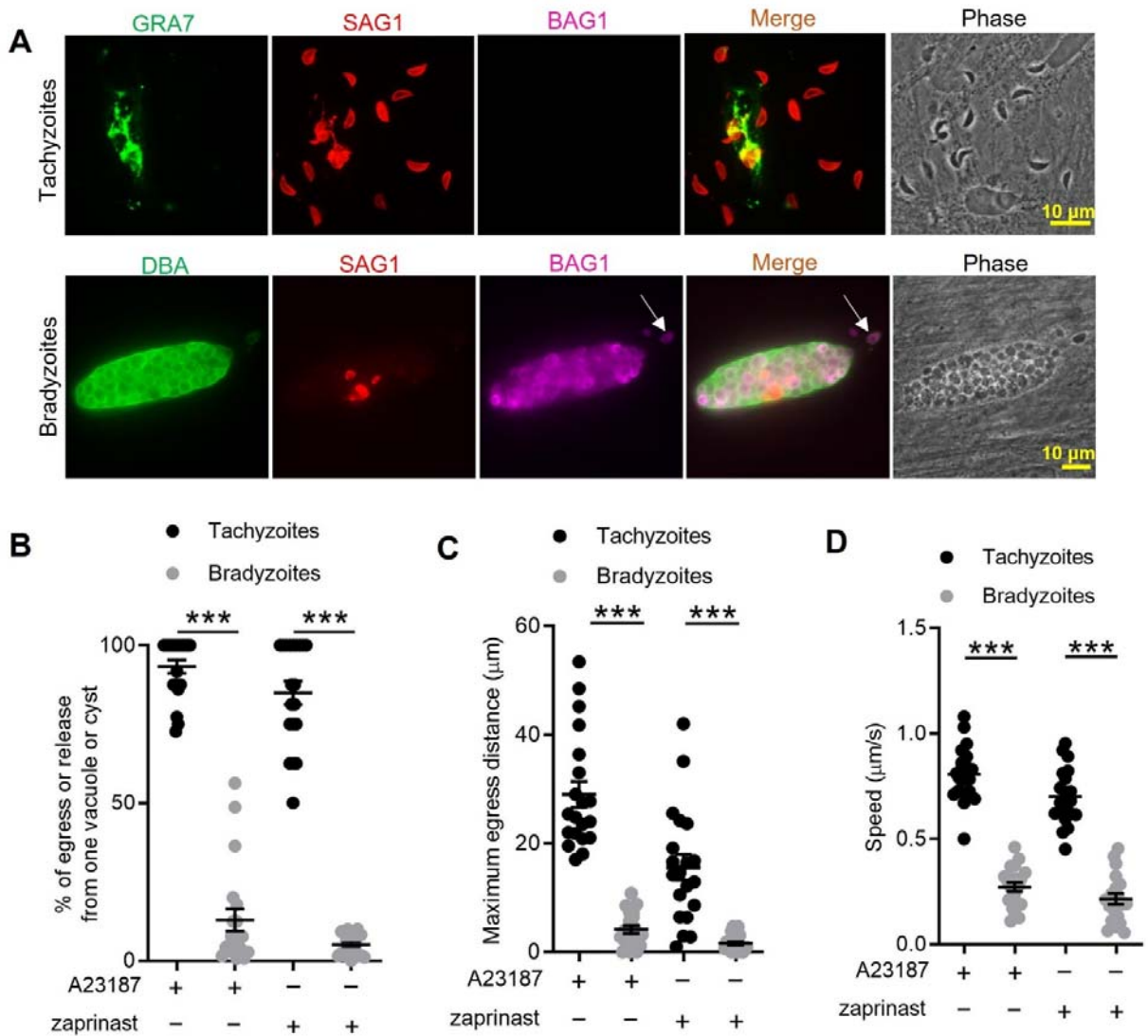
649 **Acknowledgements:** We thank Jennifer Powers Carson for technical help with the HPLC analysis which
650 was performed in the Washington University Core Laboratory for Clinical Studies. We thank Vern Carruthers
651 for providing plasmids, Louis Wiess and John Boothroyd for providing antibodies, members of the Sibley lab
652 for helpful advice, Wandy Beatty, Microbiology Imaging Facility, for technical assistance with microscopy,
653 and Jenn Barks for tissue culture support. Supported in part by a grant from the NIH (AI#034036).

654

655 **Author Contributions:** Conceived and designed the experiments: Y.F., L.D.S.; Performed the experiments: Y.F.;
656 Analyzed the data: Y.F., S.M., L.D.S.; Provided critical reagent and experimental advice: K.M.B., N.J., S.M.;
657 Supervised the work S.M., L.D.S.; Wrote the manuscript: Y.F., L.D.S.; Edited the manuscript, all authors.

658

659 **Disclosures:** The authors have no conflicts to disclose.



660

661

662

663

664

665

666

667

668

669

670

671

672

673

674

675

676

Figure 1. In vitro induced bradyzoites show limited egress in response to Ca^{2+} agonists. (A) Egress of tachyzoites and bradyzoites in response to A23187 (2 μM) for 15 min. Anti-GRA7, anti-SAG1, and anti-BAG1 antibodies followed by secondary antibodies to Alexa conjugated fluorochromes were used to detect the parasitophorous vacuole (PV) membrane, tachyzoites, and bradyzoites, respectively. DBA (*Dolichos biflorus* agglutinin) conjugated to FITC was used to stain the cyst wall. Arrow indicates released bradyzoites. Scale bar = 10 μm. (B) Quantitative analysis of egress in response to A23187 (2 μM) or zaprinast (500 μM) in extracellular buffer (EC) with Ca^{2+} for 15 min. Each data point represents the % of egressed or released parasites from one parasitophorous vacuole (PV) or cyst (n=20). Means ± SD of two independent experiments with 20 replicates. Two-tailed Mann-Whitney test, *** $P < 0.001$. (C) Quantitative analysis of maximum distance egressed or released parasites moved away from the vacuole/cyst in response to A23187 (2 μM) or zaprinast (500 μM) in EC buffer with Ca^{2+} for 15 min. Each data point represents distance travelled of one egressed tachyzoite or released bradyzoite from the original PV or cyst (n=20). Means ± SD of two independent experiments with 20 replicates. Two-tailed Mann-Whitney test, *** $P < 0.001$. (D) Quantitative analysis of speed (μm/s) of egressed or released parasites in response to A23187 (2 μM) or zaprinast (500 μM) in EC buffer with calcium for 15 min by time-lapse microscopy. Mean speed was determined by time lapse recording during the first 1 min after egress or release. Each data point represents migration speed of a single

677 egressed tachyzoites or released bradyzoites from original PV or cyst (n=20). Means \pm SD of two independent
 678 experiments with 20 replicates. Two-tailed unpaired Student's t test, *** $P < 0.001$.
 679
 680

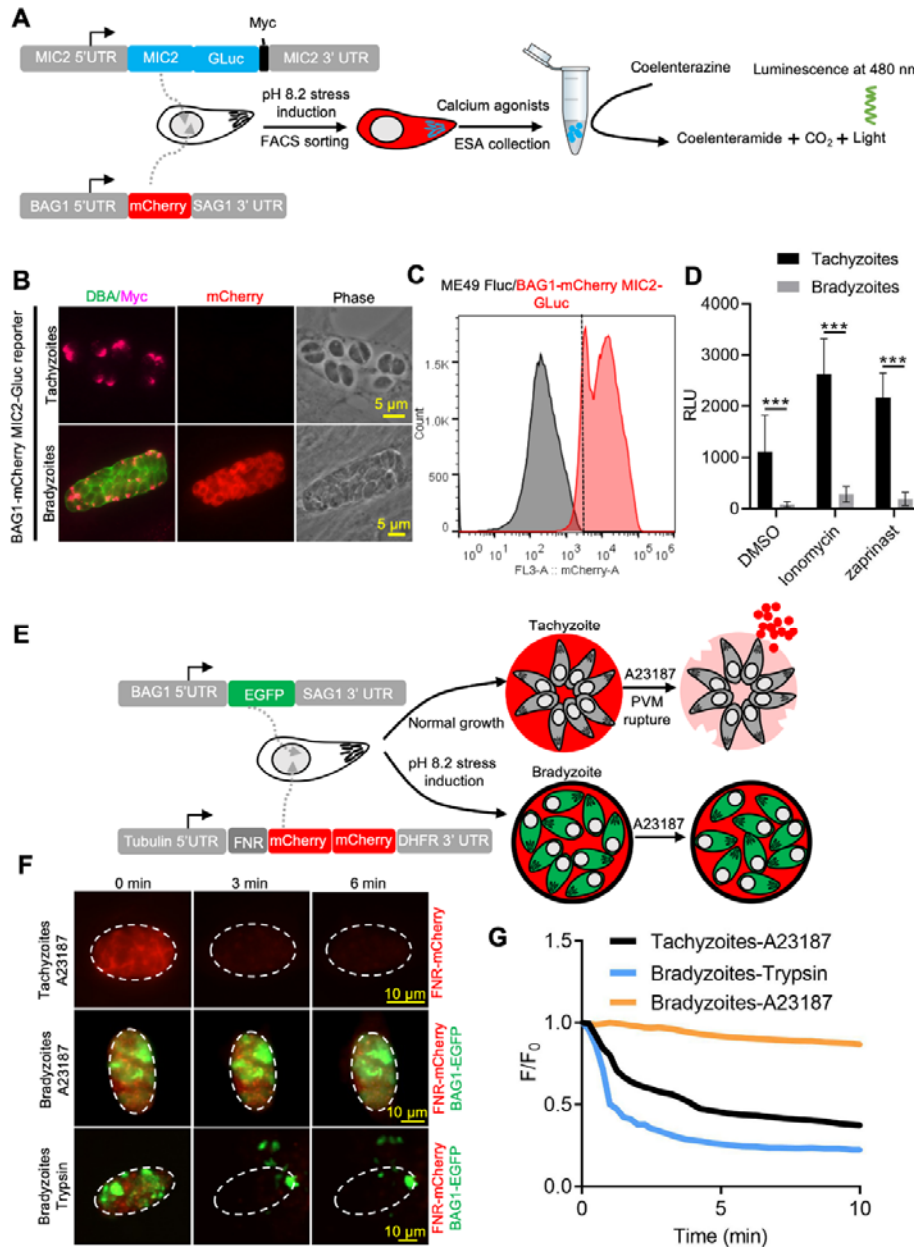


Figure 2. Ca²⁺

681
 682 **dependent microneme secretion is significantly dampened in bradyzoites.** (A) Schematic of bradyzoites
 683 MIC2 secretion assay using ME49 BAG1-mCherry MIC2-GLuc bradyzoites, differentiated in vitro by
 684 cultivation at pH 8.2 for 7 days, based on fluorescence-activated cell sorting (FACS). (B) IFA analysis
 685 showing localization of MIC2-Gluc in bradyzoites induced for 7 days at pH 8.2. MIC2-Gluc was stained with
 686 anti-Myc antibody, bradyzoites were detected with anti-mCherry, followed by secondary antibodies
 687 conjugated with Alexa Fluor dyes, and the cyst wall was stained with DBA-FITC. Bar = 5 μ m. (C)
 688 Bradyzoites expressing BAG1-mCherry were induced for 7 days at pH 8.2, mechanically liberated from cysts
 689 by 0.25 mg/ml trypsin for 5 min in intracellular buffer (IC buffer) and collected by FACS after gating with

690 parental ME49 *Δhxprt::Fluc* parasites. (D) ME49 BAG1-mCherry MIC2-Gluc tachyzoites or bradyzoites
691 sorted by FACS and resuspended in EC buffer with calcium were stimulated by 0.1% DMSO, ionomycin (1
692 μM) or zaprinast (500 μM) for 10 min at 37 °C. Release of MIC2-GLuc in ESA was determined using a
693 *Gaussia* luciferase assay. Means \pm SEM of three independent experiments each with 3 replicates. Multiple
694 Student's t tests, *** $P < 0.001$. (E) Schematic illustration of the FNR-mCherry BAG1-EGFP dual
695 fluorescence reporter and leakage of FNR-mCherry from the PV (top) or cyst matrix (bottom) following
696 A23187-induced membrane permeabilization. (F) FNR-mCherry leakage was monitored by time-lapse
697 imaging of FNR-mCherry after A23187 (2 μM) treatment. FNR-mCherry BAG1-EGFP tachyzoites cultured
698 under normal condition for 24 hr or bradyzoites induced for 7 days at pH 8.2 were treated with A23187 (2 μM)
699 or 0.25 mg/ml trypsin in EC buffer with calcium for 10 min at 37°C. Dash circle indicates the region of interest
700 (ROI) for measurement of fluorescence intensity. Bar= 10 μm . (G) FNR-mCherry fluorescence (F) over the
701 initial signal (F_0) vs. time from cells treated as in F. Curves are the mean data of 3 independent vacuoles or
702 cysts. Bradyzoites treated with DMSO group was used to assess photobleaching of mCherry (grey line).
703

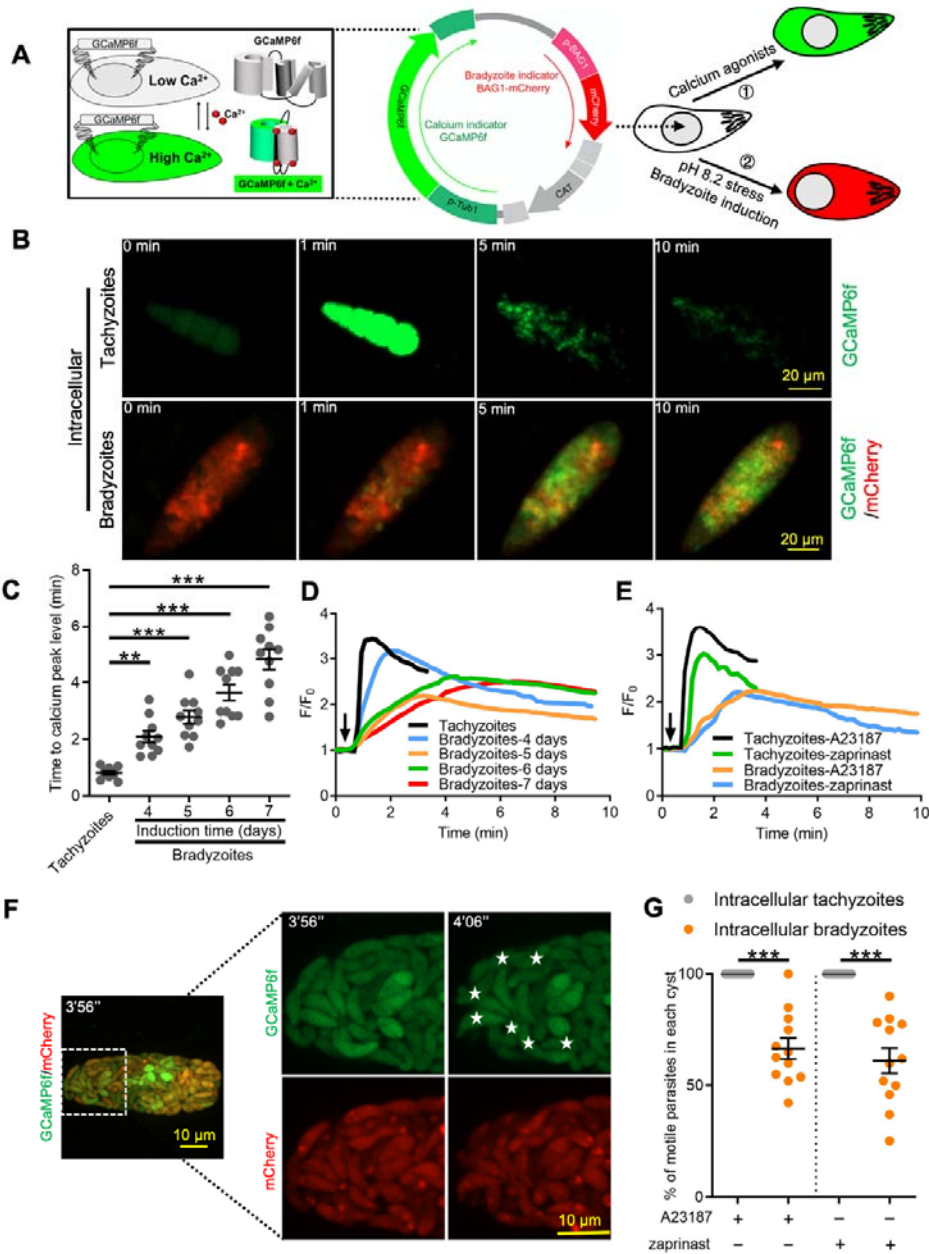


Figure 3. Ca^{2+}

704

705 **signaling is dampened during in vitro bradyzoite development induced by alkaline pH.** (A) Schematic of

706 generation of BAG1-mCherry and GCaMP6f dual fluorescent reporter to monitor Ca^{2+} responses in

707 bradyzoites. (B) Time-lapse images BAG1-mCherry GCaMP6f tachyzoites cultured for 24 hr vs. bradyzoites

708 induced for 7 days at pH 8.2 in response to A23187 (2 μ M) in EC buffer with Ca^{2+} for 10 min. Bar= 20 μ m.

709 (C) Time for reaching Ca^{2+} peak level in response to A23187 (2 μ M) for BAG1-mCherry GCaMP6f

710 expressing tachyzoites and bradyzoites induced at pH 8.2. Data points of each group represent 10 cysts or

711 vacuoles. Means \pm SD of two independent experiments with 10 replicates each. One way ANOVA with

712 Dunn's multiple comparison correction test **, $P < 0.01$, ***, $P < 0.001$. (D) Monitoring the relative intensity

713 of GCaMP fluorescence fold change (F/F_0) vs. time for intracellular tachyzoites and in vitro induced

714 bradyzoites induced at pH 8.2. Cells were treated with A23187 (2 μ M) in EC buffer without Ca^{2+} for 10 min.

715 Curves are the mean fluorescence intensity of 3 vacuoles or cysts. Arrow indicates time of addition of A23187.

716 (E) Monitoring the relative intensity of GCaMP fluorescence vs. time for intracellular tachyzoites and in vitro
717 induced bradyzoites (5 days at pH 8.2). Cells were treated with A23187 (2 μ M) or zaprinast (500 μ M) in EC
718 buffer with Ca^{2+} . Arrow indicates time of addition of agonists. Curves represent the mean data of 3
719 independent cysts or vacuoles. (F) Live time-lapse imaging of BAG1-mCherry GCaMP6f bradyzoites induced
720 for 7 days at pH 8.2 in response to A23187 (2 μ M) in EC buffer with calcium. Cells were imaged by spinning
721 disc confocal microscopy after reaching calcium peak levels (left panel). Right panel showed its
722 corresponding zoomed-in images. The interval between two continuous images is 10 s, white asterisks in the
723 latter image (4'06'') indicate motile bradyzoites by comparison with the former image (3'56''). Bar= 10 μ m.
724 (G) Motility of parasites within PVs or cysts was analyzed by time-lapse spinning disc confocal microscopy
725 and tracking of individual parasites for 5 min after reaching Ca^{2+} peak levels in response to A23187 (2 μ M) or
726 zaprinast (500 μ M) in EC buffer with calcium. Each data point represents parasites from one vacuole or cyst
727 (n=10). Data come from two independent experiments. Two-tailed Mann-Whitney test, *** $P < 0.001$. Lines
728 and error bars represent means \pm SD of two independent experiments with 10 replicates each.

729

730

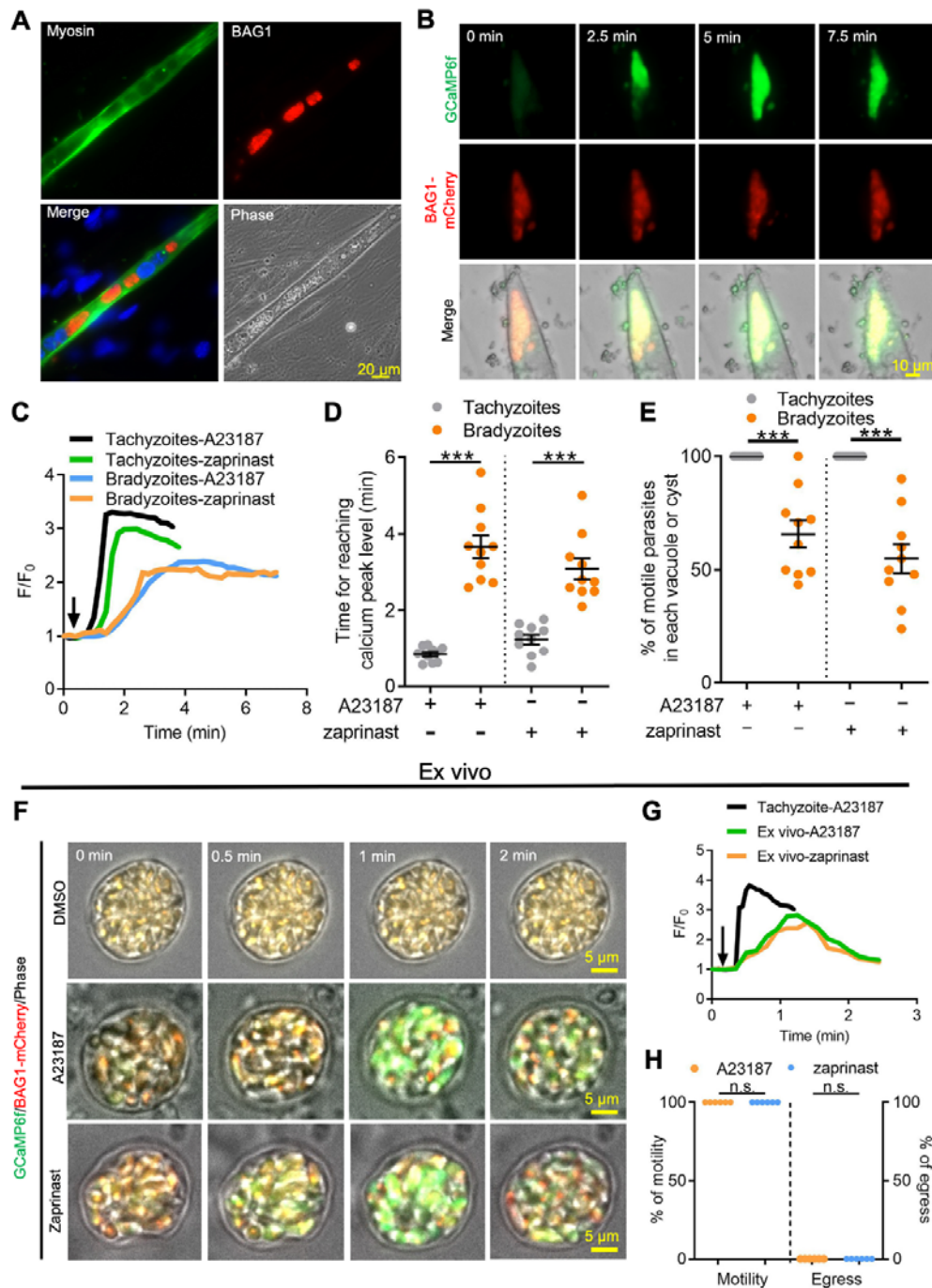


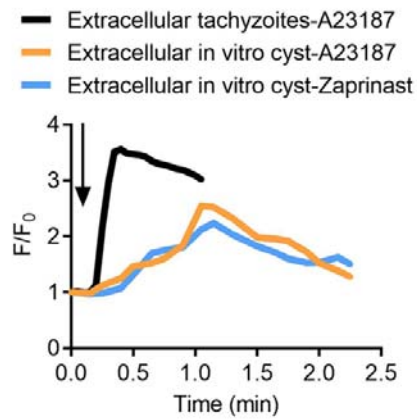
Figure 4. Ca^{2+}

731

732 **signaling is dampened in in vitro bradyzoites from spontaneously formed cysts in C2C12 muscle cells**
 733 **and cysts isolated from chronically infected mice. (A)** Microscopy based assay for detection of bradyzoites
 734 naturally formed after 7 days culture of the BAG1-mCherry GCaMP6f expressing dual reporter strain in
 735 differentiated C2C12 muscle cells. Anti-myosin antibody was used to confirm the differentiation of C2C12
 736 cells while BAG1 was used to detect bradyzoites followed by secondary antibodies conjugated with Alexa
 737 Fluor dyes. Bar = 20 μm . (B) Time-lapse recording of GCaMP6f fluorescence intensity from cysts of the
 738 BAG1-mCherry GCaMP6f strain naturally formed after 7 days culture in C2C12 cells. Cells were treated with
 739 A23187 (2 μM) in EC buffer with Ca^{2+} . Bar = 10 μm . (C) GCaMP6f fluorescence intensity changes vs. time
 740 from tachyzoites cultured in undifferentiated myoblasts or cysts naturally formed after 10 days in

741 differentiated C2C12 cells in response to A23187 (2 μ M) or zaprinast (500 μ M) in EC buffer with calcium.
742 Curves represent mean data of 3 independent cysts or vacuoles. (D) Time for reaching Ca^{2+} peak levels in
743 tachyzoites cultured in undifferentiated myoblasts and bradyzoites formed after 10 days culturing in C2C12
744 cells. Cells were treated with A23187 (2 μ M) or zaprinast (500 μ M) in EC buffer with calcium for 10 min.
745 Data points of each group come from 10 cysts or vacuoles of two independent experiments. Two-tailed
746 unpaired Student's t test, *** $P < 0.001$. Lines represent means \pm SD of two independent experiments with 10
747 replicates each. (E) Motility of parasites analyzed by time-lapse spinning disc confocal microscopy and
748 tracking of individual parasites for 5 min after reaching calcium peak levels in response to A23187 (2 μ M) or
749 zaprinast (500 μ M) in EC buffer with calcium. Lines represent means \pm SD of two independent experiments
750 with 10 replicates each. Two-tailed Mann-Whitney t test, *** $P < 0.001$. (F) Monitoring of GCaMP
751 fluorescence in response to 0.1% DMSO, A23187 (2 μ M) or zaprinast (500 μ M) in EC buffer with Ca^{2+} in ex
752 vivo cysts isolated from the brains of mice infected with BAG1-mCherry GCaMP6f reporter parasites. Cysts
753 were harvested at 30 days post infection. Bar = 5 μ m. (G) GCaMP6f fluorescence intensity changes vs. time
754 within BAG1-mCherry GCaMP6f ex vivo cysts in response to A23187 (2 μ M) or zaprinast (500 μ M) in EC
755 buffer with calcium. Curves are the mean data of 3 independent cysts. (H) Quantitative analysis of motility
756 and egress by bradyzoites from ex vivo cysts isolated from CD-1 mice brain tissues at 30 days post-infection.
757 Motility was analyzed by time-lapse microscopy and tracking of individual parasites using time points similar
758 to D, E above. Each data point represents percentage of motile or egressed parasites from one cyst (n=5).
759 Significance was determined by two-tailed Student's t-test, n.s., not significant.

760

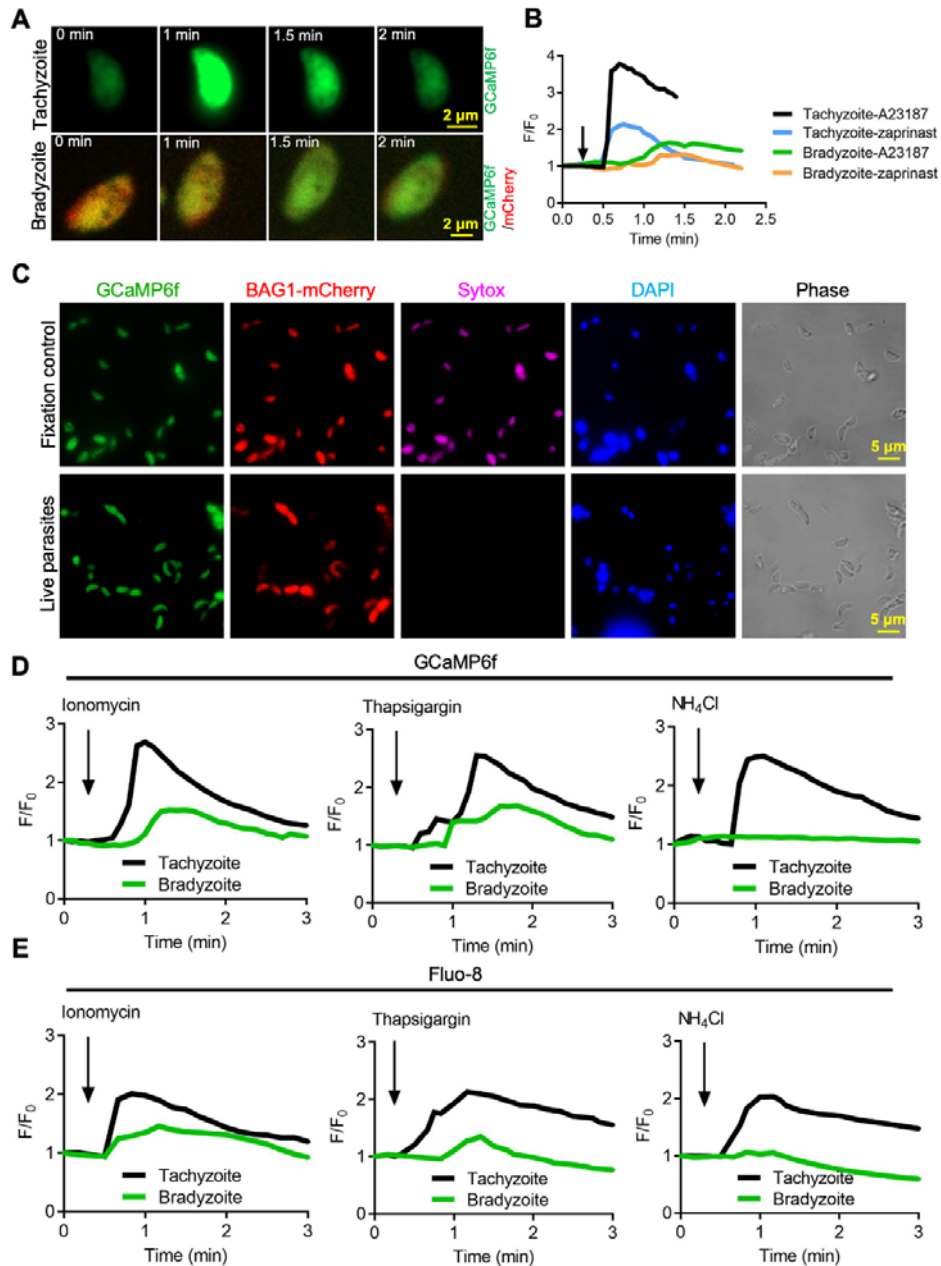


761

762 **Figure 4 figure supplement 1 Calcium responses by extracellular tachyzoites and in vitro produced**
763 **tissue cysts**

764 (A) Fluorescence recording of ME49 strain parasites expressing GCaMP6f in response to A23187 (2 μ M) or
765 zaprinast (500 μ M). Freshly harvested extracellular tachyzoites were compared to cysts induced in vitro in pH
766 8.2 RPMI 1640 medium for 7 days. Arrow indicates time of addition of calcium agonists. Each kinetic curve
767 represented the mean of 3 independent samples.

768



769

770 **Figure 5. Bradyzoites have lower Ca²⁺ stores and reduced responses to agonists compared to tachyzoites.**

771 (A) Live imaging of extracellular BAG1-mCherry GCaMP6f dual fluorescent reporter tachyzoites and

772 bradyzoites induced for 7 days at pH 8.2 in response to A23187 (2 μM) in EC buffer with Ca²⁺. Bar= 2 μm. (B)

773 Fluorescence recording of increased GCaMP6f fluorescence with Ca²⁺ increase in response to A23187 (2 μM)

774 or zaprinast (500 μM) in EC buffer with Ca²⁺ for extracellular tachyzoites and bradyzoites. Arrow indicates

775 the addition of calcium agonists. Each curve is the mean of three individual parasites. (C) BAG1-mCherry

776 GCaMP6f reporter live bradyzoites were stained by SYTOXTM far red to detected dead cells and DAPI 30 min

777 after liberation from cysts. Formaldehyde-fixed bradyzoites serve as positive control. Bar= 5 μm. (D)

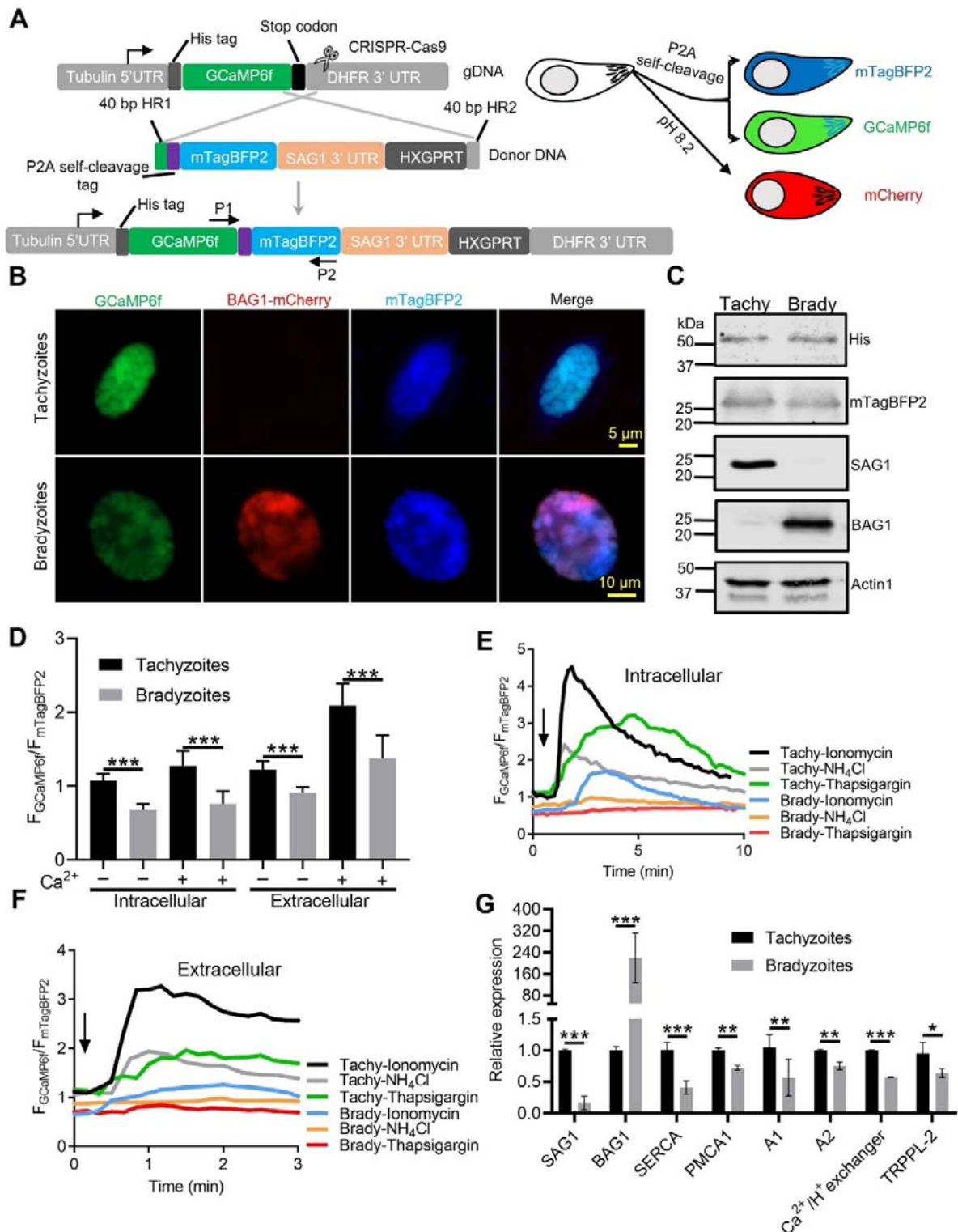
778 GCaMP6f fluorescence intensity vs. time for extracellular BAG1-mCherry GCaMP6f dual reporter parasites

779 in response to 1 μM ionomycin, 1 μM thapsigargin, or 10 mM NH₄Cl in EC buffer without Ca²⁺. Arrow

780 indicates the addition of agonist. Each curve is the mean of three individual parasites. (E) Fluorescence

781 intensities change fold vs. time of extracellular BAG1-mCherry expressing bradyzoites loaded with 500 nM
782 Fluo-8 AM after addition of 1 μ M ionomycin, 1 μ M thapsigargin or 10 mM NH_4Cl in EC buffer without Ca^{2+} .
783 Arrow indicates the addition of agonist. Each curve is the mean of three individual parasites.

784



785

786 **Figure 6. Ratiometric Ca²⁺ imaging of bradyzoites reveals lower levels of resting Ca²⁺ and reduced**

787 **response to Ca²⁺ ionophores compared to tachyzoites.** (A) Schematic diagram of generation of a

788 ratiometric calcium reporter containing GCaMP6f fused with by a peptide P2A and blue fluorescence

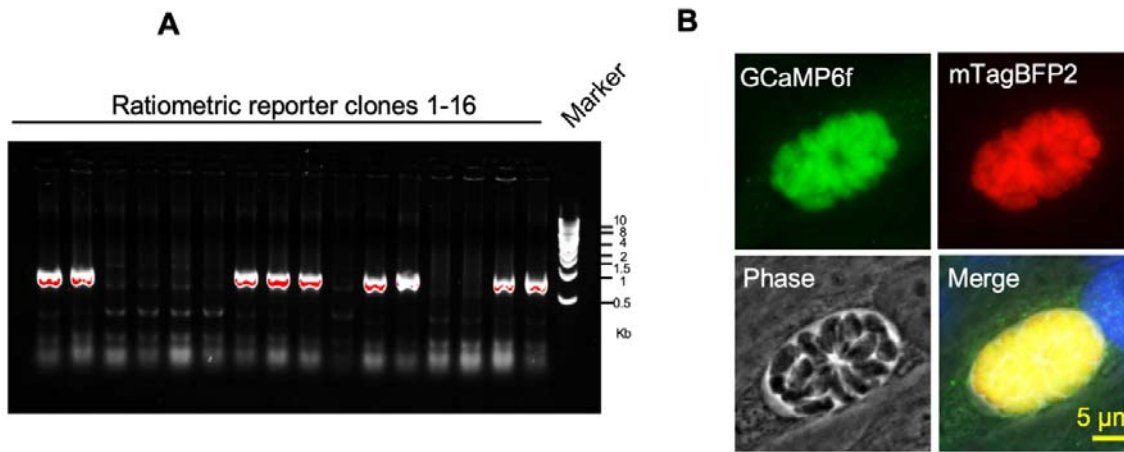
789 indicator mTagBFP2 in the background of BAG1-mCherry reporter strain. (B) Fluorescence microscopy

790 imaging of intracellular ratiometric indicator expressed by tachyzoites cultured for 24 hr vs. bradyzoites

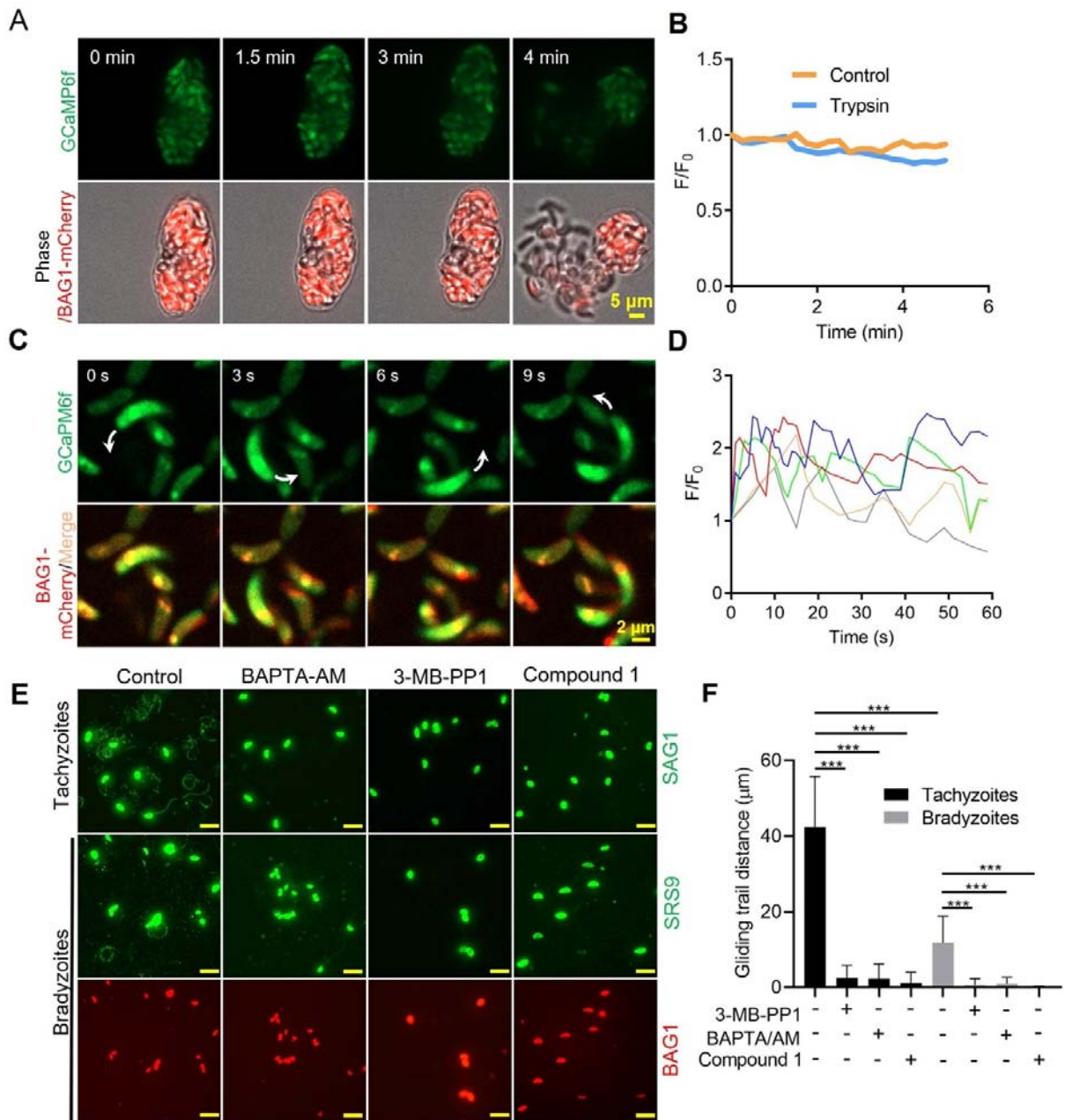
791 induced for 7 days at pH 8.2 culture in EC buffer without Ca²⁺. Bar= 10 μm. (C) Western blots showing

792 GCaMP6f and mTagBFP2 produced from the ratiometric reporter expressed by tachyzoites and bradyzoite.
793 α His and α tRFP antibodies were used to probe the expression of GCaMP6f and mTagBFP2, respectively.
794 SAG1 and BAG1 serve as the stage-specific marker of tachyzoites and bradyzoites, respectively. Actin
795 functions as loading control. (D) Quantification of basal calcium levels normalized by comparison of
796 GCaMP6f to mTagBFP2 fluorescence intensity ratios of intracellular and extracellular tachyzoites or
797 bradyzoites that were induced by culture for 7 days at pH 8.2. For extracellular parasites, tachyzoites were
798 liberated mechanically and bradyzoites were liberated by trypsin treatment. Parasites within intact cells, or
799 extracellular parasites were incubated in EC buffer with or without Ca^{2+} for 10 min before imaging. Data
800 represent mean values from two independent experiments with 10 total vacuoles or cysts for each treatment.
801 Two-tailed unpaired Student's t test, ***, $P < 0.001$. (E) Monitoring of GCaMP6f/ mTagBFP2 fluorescence
802 intensity ratio vs. time for intracellular tachyzoites and in vitro induced bradyzoites that were induced by
803 culture for 7 days at pH 8.2. (F) For extracellular parasites, tachyzoites were liberated mechanically and
804 bradyzoites were liberated by trypsin treatment. Parasites were incubated in EC buffer without Ca^{2+} for 10
805 min and responses were measured to ionomycin (1 μM), thapsigargin (1 μM) or 10 mM NH_4Cl . Arrow
806 indicates time of addition of agonists. Each kinetic curve represents mean data of 3 independent samples
807 (individual vacuoles or cysts for intracellular and single parasites for extracellular). (G) Gene expression
808 levels in tachyzoites and bradyzoites induced for 7 days at pH 8.2. mRNA levels were measured using
809 RT-PCR and expressed relative to the housekeeping transcript for actin. SAG1 and BAG1 were used to
810 monitor tachyzoites and bradyzoites, respectively. Data represent the mean \pm SD of two independent assays
811 containing triplicate samples each. Multiple Student's t tests, **, $P < 0.01$, ***, $P < 0.001$.

812



813
814 **Figure 6 figure supplement 1 Identification of ME49 GCaMP6f-P2A-mTagBFP2 BAG1-mCherry**
815 **ratiometric reporter by PCR and IFA**
816 (A) Transgenic screening of clones of ME49 GCaMP6f BAG1-mCherry parasites expressing P2A-mTagBFP2
817 at the C-terminal of GCaMP6f using PCR amplification with primer set P1-P2 shown in diagram in **Figure**
818 **6A**. (B) IFA analysis showing co-localization of GCaMP6f and mTagBFP2 in tachyzoites of the dual reporter
819 strain grown in HFF cells for 24 hr. Monoclonal anti-His antibody was used to stain GCaMP6f while rabbit
820 anti-tRFP antibody was used to stain mTagBFP2 followed by goat anti-mouse IgG conjugated to Alexa
821 Fluor-488 and goat anti-rabbit IgG conjugated to Alexa Fluor-568 secondary antibodies. Scale bar = 5 μ m.
822

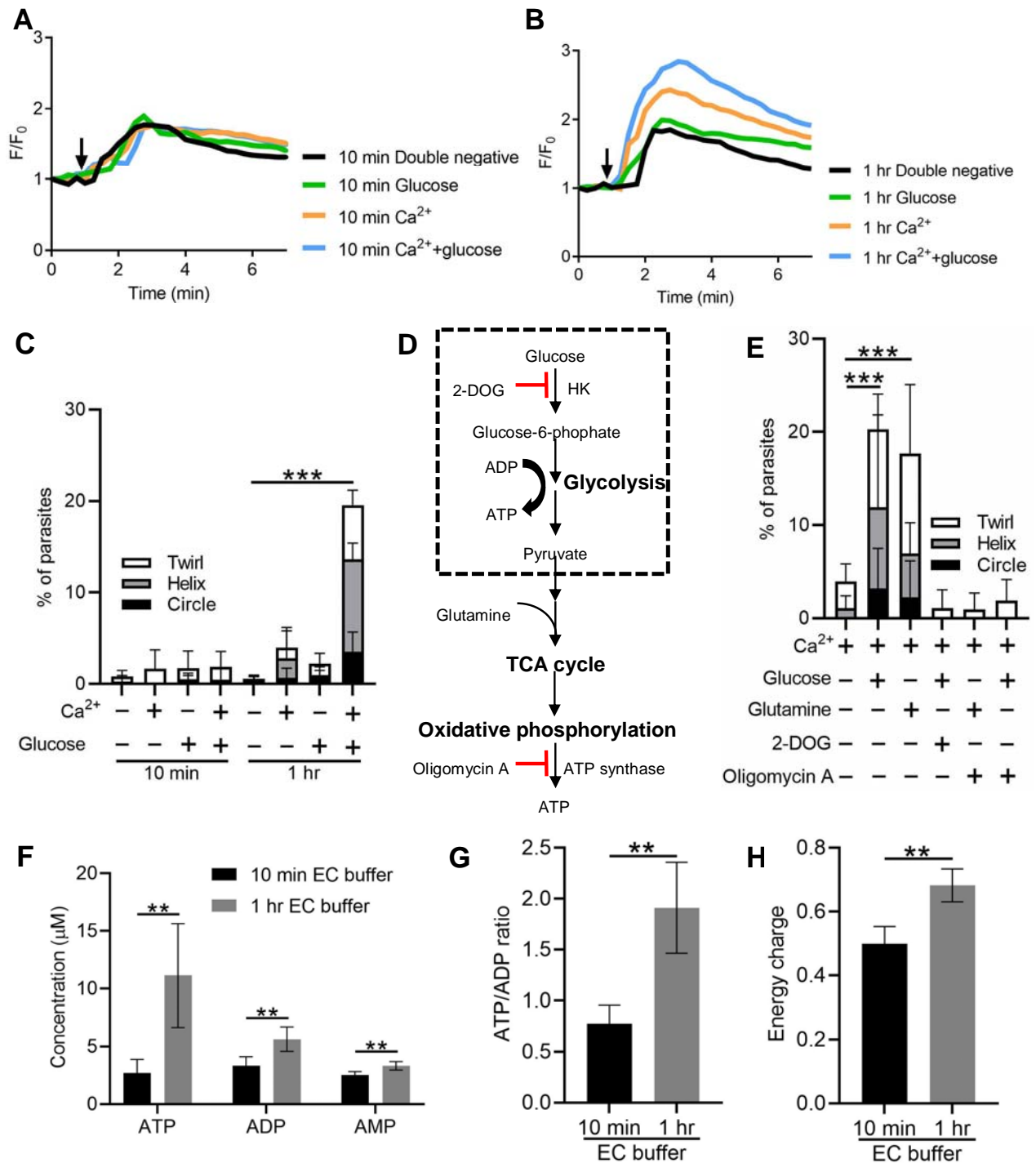


823

824 **Figure 7. Ca²⁺ signaling governs gliding motility of bradyzoites.** (A) Time-lapse microscopy recording
 825 GCaMP6f BAG1-mCherry bradyzoites induced for 7 days at pH 8.2. Cells were imaged during the digestion
 826 by 0.25 mg/ml Trypsin for 5 min in EC buffer with 1.8 mM Ca²⁺. Bar = 5 μ m. (B) GCaMP6f fluorescence
 827 change ratio vs. time of BAG1-mCherry GCaMP6f bradyzoites induced for 7 days at pH 8.2 treated with or
 828 without trypsin. Curves represent mean data from 3 independent cysts. (C) Spinning disc confocal microscopy
 829 monitoring circular gliding motility of bradyzoites liberated by 0.25 mg/ml trypsin for 10 min from cysts
 830 induced for 7 days at pH 8.2. Arrow shows the direction of gliding motility by one bradyzoite. Bar = 5 μ m. (D)
 831 Ca²⁺ kinetics of bradyzoites undergoing gliding motility after liberation from cysts induced for 7 days at pH
 832 8.2. The graph shows fluctuated Ca²⁺ kinetics of 5 independent single bradyzoites. (E) Indirect
 833 immunofluorescence microscopy showing the trails of parasites during gliding motility. Parasites were treated
 834 with DMSO (control), 5 μ M 3-MB-PP1, 25 μ M BAPTA-AM and 4 μ M Compound 1. Anti-SAG1 mAb DG52

835 and rabbit polyclonal anti-SRS9 antibodies followed by secondary antibodies conjugated to goat anti-mouse
836 IgG Alexa 488 were used to stain the gliding trails of tachyzoites and bradyzoites, respectively. Anti-BAG1
837 followed by goat anti-rabbit IgG conjugated of Alexa 568 served as marker of bradyzoites. Bar=10 μm . (F)
838 Quantification of trails from gliding motility of tachyzoites and bradyzoites treated with DMSO (control), 5
839 μM 3-MB-PP1, 25 μM BAPTA-AM and 4 μM compound 1. Data represented as means \pm SEM ((n = 20
840 replicates combined from n = 3 independent experiments). Kruskal-Wallis test with Dun's multiple
841 comparison correction ***, $P < 0.001$.

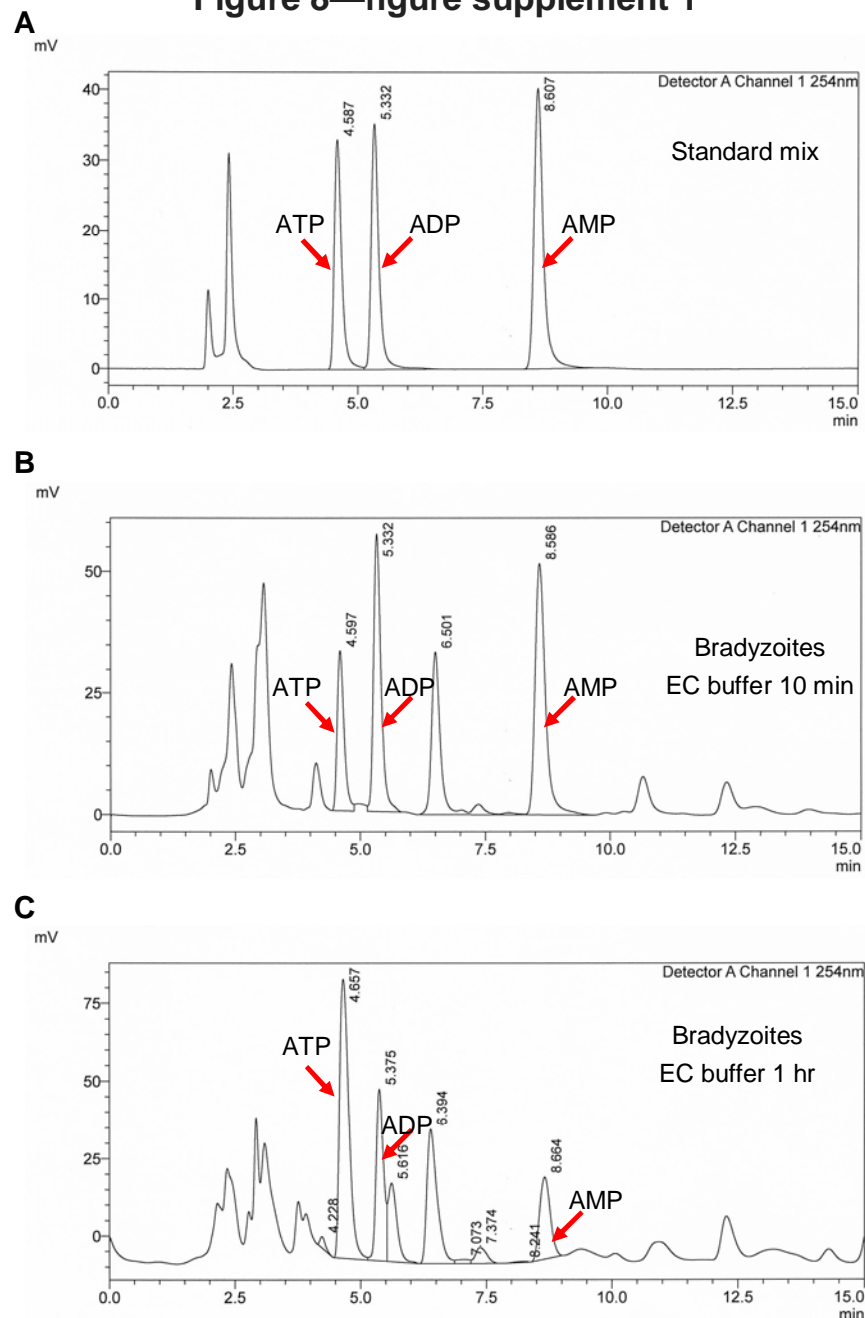
842



843 **Figure 8. Exogenous Ca^{2+} and glucose collectively contributes to bradyzoites gliding motility via**
 844 **refilling calcium pools and increasing ATP production.** (A-B) Monitoring the relative intensity of
 845 GCaMP6f fluorescence fold change (F/F_0) vs. time from extracellular bradyzoites treated with $1 \mu\text{M}$
 846 ionomycin. Bradyzoites induced for 7 days at pH 8.2 were released from in vitro cysts by 0.25 mg/ml trypsin
 847 and pre-incubated in EC buffer $\pm 1.8 \text{ mM}$ Ca^{2+} and/or $\pm 5.6 \text{ mM}$ glucose for 10 min (A) or 1 hr (B) before
 848 measurements. Each kinetic curve represents mean data of 3 extracellular parasites. Arrow indicates the
 849 addition of $1 \mu\text{M}$ ionomycin. Double negative refers to the absence of Ca^{2+} and glucose. (C) Percentage of

850 extracellular parasites undergoing different forms of gliding motility as determined from time-lapse video
851 microscopy. Bradyzoites induced for 7 days at pH 8.2 were treated in EC buffer \pm 1.8 mM Ca^{2+} and/or \pm 5.6
852 mM glucose for 10 min or 1 hr before measurements. Means \pm SD of two independent experiments with 6
853 replicates each. Kruskal-Wallis test with Dunn's multiple comparison correction test ***, $P < 0.001$ for
854 comparison between - calcium / - glucose and + calcium / + glucose. All other groups were not significantly
855 different from the negative control. (D) Schematic illustration of mechanism of 2-deoxyglucose (2-DOG) and
856 oligomycin A in inhibiting ATP production. (E) Percentage of bradyzoites with different forms of gliding
857 motility determined by time-lapse video microscopy. Bradyzoites induced for 7 days at pH 8.2 were treated in
858 EC buffer (1.8 mM Ca^{2+}) \pm 5.6 mM glucose, 5.6 mM glutamine, 50 mM 2-DOG, or 20 μM oligomycin A for
859 1 hr before measurements. Means \pm SD of two independent experiments with 6 replicates each.
860 Kruskal-Wallis test with Dunn's multiple comparison correction test ***, $P < 0.001$. (F-H) High-performance
861 liquid chromatography UV (HPLC-UV) analysis of ATP, ADP and AMP levels in extracellular bradyzoites
862 incubated with EC buffer containing 1.8 mM Ca^{2+} and 5.6 mM glucose for 10 min or 1 hr. Bradyzoites induced
863 for 7 days at pH 8.2 were purified by magnetic beads and released from in vitro cysts by 0.25 mg/ml trypsin.
864 Data from two independent experiments with 6 technical replicates. (F) Concentrations of ATP, ADP, and AMP
865 in extracellular bradyzoites represented as mean \pm SD. Multiple Student's t tests, **, $P < 0.01$. (G) ATP/ADP
866 ratios in extracellular bradyzoites represented as mean \pm SD. Two-tailed Mann-Whitney test, **, $P < 0.01$. (H)
867 Energy charge of extracellular bradyzoites calculated as $[\text{ATP}] + 0.5[\text{ADP}] / [\text{ATP}] + [\text{ADP}] + [\text{AMP}]$ represented
868 as mean \pm SD Two-tailed Mann-Whitney test, **, $P \leq 0.01$.

Figure 8—figure supplement 1



869 **Figure 8 figure supplement 1 Establishment of HPLC-UV analysis of ATP, ADP and AMP levels in**
870 **parasites**

871 (A) HPLC-UV chromatograms of standard mix containing 12.5 μ M ATP, 12.5 μ M ADP and 12.5 μ M AMP.
872 Arrows indicate the peaks of ATP, ADP and AMP. (B) HPLC-UV chromatograms of ATP, ADP and AMP
873 extracts from bradyzoites (2×10^7) incubated with EC buffer containing 1.8 mM Ca^{2+} and 5.6 mM glucose for
874 10 min. Arrows indicate the peaks of ATP, ADP and AMP. (C) HPLC-UV chromatograms of ATP, ADP and
875 AMP extracts from bradyzoites (1.2×10^7) incubated with EC buffer containing 1.8 mM Ca^{2+} and 5.6 mM
876 glucose for 1 hr. Arrows indicate the peaks of ATP, ADP and AMP.

877

878 **Rich Media Files**

879 **Figure 1-video 1 Egress by ME49 BAG1-mCherry tachyzoites in response to A23187.**

880 Time-lapse video microscopy showing A23187 (2 μ M) induced egress of ME49 BAG1-mCherry strain
881 tachyzoites grown in vitro in HFF cells for 24 hr. Videos for intracellular tachyzoites in EC buffer were
882 recorded for 10 min and A23187 (2 μ M) was added 30 s after the recording initiated. Display frame rate is 8
883 frames per second while the acquisition frame rate is 3 frames per second. Bar = 10 μ m.

884 **Figure 1-video 2 Egress by ME49 BAG1-mCherry bradyzoites in response to A23187.**

885 Time-lapse video microscopy showing A23187 (2 μ M) induced egress of ME49 BAG1-mCherry strain
886 bradyzoites induced by in vitro culture on HFF cells for 7 days at pH 8.2. Videos for intracellular bradyzoites
887 in EC buffer were recorded for 10 min and A23187 (2 μ M) was added 30 s after the recording initiated.
888 Display frame rate is 4 frames per second while the acquisition frame rate is 10 frames per second. Bar = 10
889 μ m.

890 **Figure 2-video 1 A23187 - induced permeabilization of the parasitophorous vacuole membrane (PVM)**
891 **detected by vacuolar leakage of FNR-mCherry secreted by tachyzoites.**

892 Time-lapse video microscopy showing A23187 (2 μ M)-induced FNR-mCherry leakage from the PV
893 surrounding FNR-mCherry BAG1-EGFP expressing tachyzoites. FNR-mCherry BAG1-EGFP tachyzoites
894 cultured under normal condition in HFF cells for 24 hr were treated with A23187 (2 μ M) in EC buffer for 10
895 min at 37°C. Videos were recorded for 10 min and A23187 (2 μ M) was added 30 s after the recording initiated.
896 Display frame rate is 6 frames per second while the acquisition frame rate is 5 frames per second. Bar = 5 μ m.

897 **Figure 2-video 2 Trypsin - induced disruption of in vitro differentiated tissue cysts expressing ME49**
898 **FNR-mCherry BAG1-EGFP.**

899 Time-lapse video microscopy showing A23187-induced FNR-mCherry leakage in vitro differentiated tissue
900 cysts of FNR-mCherry BAG1-EGFP bradyzoites. FNR-mCherry BAG1-EGFP bradyzoites induced by
901 cultivation in HFF cells in vitro for 7 days at pH 8.2 were treated with 0.25 mg/ml Trypsin in EC buffer for 6
902 min at 37°C. Videos were recorded for 6 min and 0.25 mg/ml Trypsin was added 30 s after the recording
903 initiated. Display frame rate is 3 frames per second while the acquisition frame rate is 15 frames per second.
904 Bar = 5 μ m.

905 **Figure 2-video 3 A23187 -induced permeabilization of in vitro differentiated tissue cysts detected by**
906 **vacuolar FNR-mCherry leakage from ME49 FNR-mCherry BAG1-EGFP bradyzoites.**

907 Time-lapse video microscopy showing A23187 (2 μ M)-induced FNR-mCherry leakage from in vitro
908 differentiated cysts of FNR-mCherry BAG1-EGFP. FNR-mCherry BAG1-EGFP bradyzoites induced by
909 cultivation in HFF cells in vitro for 7 days at pH 8.2 were treated with A23187 (2 μ M) in EC buffer for 10 min
910 at 37°C. Videos were recorded for 10 min and A23187 (2 μ M) was added 30 s after the recording initiated.
911 Display frame rate is 3 frames per second while the acquisition frame rate is 15 frames per second. Bar = 5
912 μ m.

913 **Figure 3-video 1 Calcium response of ME49 BAG1-Cherry GCaMP6f expressing tachyzoites stimulated**
914 **by A23187.**

915 Time-lapse video microscopy showing GCaMP6f fluorescence changes of intracellular ME49 BAG1-mCherry
916 GCaMP6f tachyzoites grown in HFF cells in vitro for 24 hr in response to A23187 (2 μ M) in EC buffer.
917 Videos were recorded for 10 min and A23187 (2 μ M) was added 30 s after the recording initiated. Display
918 frame rate is 10 frames per second while the acquisition frame rate is 3 frames per second. Bar = 10 μ m.

919 **Figure 3-video 2 Calcium response of ME49 BAG1-Cherry GCaMP6f expressing bradyzoites**
920 **stimulated by A23187.**

921 Time-lapse video microscopy showing GCaMP6f fluorescence changes of intracellular ME49 BAG1-mCherry
922 GCaMP6f bradyzoites induced by cultivation in HFF cells in vitro for 7 days at pH 8.2 in response to A23187
923 (2 μ M) in EC buffer. Videos were recorded for 14 min and A23187 (2 μ M) was added 30 s after the recording
924 initiated. Display frame rate is 6 frames per second while the acquisition frame rate is 10 frames per second.
925 Bar = 10 μ m.

926 **Figure 4-video 1 Calcium response of ME49 BAG1-mCherry GCaMP6f cysts isolated from chronically**
927 **infected mouse brains and treated in vitro with DMSO.**

928 Time-lapse video microscopy showing GCaMP6f fluorescence changes of ME49 BAG1-mCherry GCaMP6f
929 cysts isolated 30 days post-infection from the brains of chronically infected mice in response to DMSO (0.1%)
930 in EC buffer. Videos were recorded for 5 min and DMSO (0.1%) was added 15 s after the recording initiated.
931 Display frame rate is 6 frames per second while the acquisition frame rate is 3 frames per second. Bar = 2 μ m.

932 **Figure 4-video 2 Calcium response of ME49 BAG1-mCherry GCaMP6f cysts isolated from chronically**
933 **infected mouse brains and treated in vitro with A23187.**

934 Time-lapse video microscopy showing GCaMP6f fluorescence changes of ME49 BAG1-mCherry GCaMP6f
935 cysts isolated 30 days post-infection from chronically infected mice in response to A23187 (2 μ M) in EC
936 buffer. Videos were recorded for 5 min and A23187 (2 μ M) was added 15 s after the recording initiated.
937 Display frame rate is 6 frames per second while the acquisition frame rate is 5 frames per second. Bar = 2 μ m.

938 **Figure 5-video 1 Calcium response of extracellular ME49 BAG1-mCherry GCaMP6f tachyzoite in**
939 **response to A23187.**

940 Time-lapse video microscopy showing GCaMP6f fluorescence changes of extracellular ME49
941 BAG1-mCherry GCaMP6f tachyzoite in response to A23187 (2 μ M) in EC buffer. Videos were recorded for 3
942 min and A23187 (2 μ M) was added 15 s after the recording initiated. Display frame rate is 4 frames per
943 second while the acquisition frame rate is 3 frames per second. Bar = 2 μ m.

944 **Figure 5-video 2 Calcium response of extracellular ME49 BAG1-mCherry GCaMP6f bradyzoite in**
945 **response to A23187.**

946 Time-lapse video microscopy showing GCaMP6f fluorescence changes of extracellular ME49
947 BAG1-mCherry GCaMP6f bradyzoite in response to A23187 (2 μ M) in EC buffer. Bradyzoites were liberated
948 by 0.25 mg/ml trypsin for 5 min from in vitro cysts induced for cultivation in HFF cells for 7 days at pH 8.2.
949 Videos were recorded for 3 min and A23187 (2 μ M) was added 15 s after the recording initiated. Display
950 frame rate is 2 frames per second while the acquisition frame rate is 5 frames per second. Bar = 2 μ m.

951 **Figure 7-video 1 Trypsin induced liberation of ME49 BAG1-mCherry GCaMP6f bradyzoites from in**
952 **vitro cultured cysts.**

953 Time-lapse video microscopy recording GCaMP6f fluorescence changes from BAG1-mCherry GCaMP6f
954 bradyzoites induced by cultivation in HFF cells for 7 days at pH 8.2 during digestion by 0.25 mg/ml Trypsin
955 in EC buffer. Videos were recorded for 6 min and 0.25 mg/ml trypsin was added 30 s after the recording
956 initiated. Display frame rate is 16 frames per second while the acquisition frame rate is 5 frames per second.
957 Bar = 5 μ m.

958 **Figure 7-video 2 Gliding motility of ME49 BAG1-mCherry GCaMP6f bradyzoites released from in**
959 **vitro cysts.**

960 Time-lapse video microscopy of gliding motility of bradyzoites liberated by 0.25 mg/ml trypsin for 5 min
961 from in vitro cyst induced by cultivation in HFF cells for 7 days at pH 8.2. Images were collected using
962 spinning disc confocal microscopy. The arrow shows the gliding motility of bradyzoite in EC buffer. Videos
963 were recorded for 2 min. Display frame rate is 6 frames per second while the acquisition frame rate is 1 frame
964 per second. Bar = 2 μ m.

965
966 **Supplementary Files**

967 Supplementary Table 1: Primers used in this study
968 Supplementary Table S2 Plasmids used in this study
969 Supplementary Table S3 Parasite lines used in this study

970

971 **References**

972

- 973 1. Dubey JP (2010) *Toxoplasmosis of animals and humans*. Boca Raton: CRC Press. 313 p.
- 974 2. Jones JL, Dubey JP (2012) Foodborne *Toxoplasmosis*. *Clin Infect Dis* 55: 864-851.
- 975 3. Jones JL, Dubey JP (2010) Waterborne *toxoplasmosis*--recent developments. *Exp Parasitol* 124: 10-25.
- 976 4. Drewry LL, Sibley LD (2019) The hitchhiker's guide to parasite dissemination. *Cell Microbiol*: e13070.
- 977 5. Watts E, Zhao Y, Dhara A, Eller B, Patwardhan A, et al. (2015) Novel Approaches Reveal that *Toxoplasma gondii*
978 Bradyzoites within Tissue Cysts Are Dynamic and Replicating Entities In Vivo. *MBio* 6: e01155-01115.
- 979 6. Jeffers V, Tampaki Z, Kim K, Sullivan WJ, Jr. (2018) A latent ability to persist: differentiation in *Toxoplasma gondii*. *Cell*
980 *Mol Life Sci* 75: 2355-2373.
- 981 7. Mayoral J, Di Cristina M, Carruthers VB, Weiss LM (2020) *Toxoplasma gondii*: Bradyzoite Differentiation In Vitro and In
982 Vivo. *Methods Mol Biol* 2071: 269-282.
- 983 8. Lourido S, Moreno SN (2015) The calcium signaling toolkit of the Apicomplexan parasites *Toxoplasma gondii* and
984 *Plasmodium* spp. *Cell Calcium* 57: 186-193.
- 985 9. Carruthers VB, Sibley LD (1999) Mobilization of intracellular calcium stimulates microneme discharge in *Toxoplasma*
986 *gondii*. *Mol Microbiol* 31: 421-428.
- 987 10. Carruthers VB, Moreno SNJ, Sibley LD (1999) Ethanol and acetaldehyde elevate intracellular [Ca²⁺] calcium and
988 stimulate microneme discharge in *Toxoplasma gondii*. *Biochem J* 342: 379-386.
- 989 11. Wetzel DM, Chen LA, Ruiz FA, Moreno SNJ, Sibley LD (2004) Calcium-mediated protein secretion potentiates motility
990 by *Toxoplasma gondii*. *J Cell Sci* 117: 5739-5748.
- 991 12. Lovett JL, Marchesini N, Moreno SN, Sibley LD (2002) *Toxoplasma gondii* microneme secretion involves intracellular
992 Ca²⁺ release from IP₃ / ryanodine sensitive stores. *J Biol Chem* 277: 25870-25876.
- 993 13. Vieira MCF, Moreno SNJ (2000) Mobilization of intracellular calcium upon attachment of *Toxoplasma gondii*
994 tachyzoites to human fibroblasts is required for invasion. *Molec Biochem Parasit* 106: 157-162.
- 995 14. Pace DA, McKnight CA, Liu J, Jimenez V, Moreno SN (2014) Calcium entry in *Toxoplasma gondii* and its enhancing
996 effect of invasion-linked traits. *J Biol Chem*.
- 997 15. Kafsack BF, Pena JD, Coppens I, Ravindran S, Boothroyd JC, et al. (2009) Rapid membrane disruption by a
998 perforin-like protein facilitates parasite exit from host cells. *Science* 323: 530-533.
- 999 16. Brown KM, Sibley LD (2018) Essential cGMP Signaling in *Toxoplasma* Is Initiated by a Hybrid P-Type
1000 ATPase-Guanylate Cyclase. *Cell Host Microbe* 24: 804-816 e806.
- 1001 17. Bisio H, Lunghi M, Brochet M, Soldati-Favre D (2019) Phosphatidic acid governs natural egress in *Toxoplasma gondii*
1002 via a guanylate cyclase receptor platform. *Nat Microbiol* 4: 420-428.
- 1003 18. Yang L, Uboldi AD, Seizova S, Wilde ML, Coffey MJ, et al. (2019) An apically located hybrid guanylate cyclase-ATPase
1004 is critical for the initiation of Ca(2+) signaling and motility in *Toxoplasma gondii*. *J Biol Chem* 294: 8959-8972.
- 1005 19. Brown KM, Long S, Sibley LD (2017) Plasma membrane association by N-acylation governs PKG function in
1006 *Toxoplasma gondii*. *mBio* 8(3): e00375-00317.
- 1007 20. Fang J, Marchesini N, Moreno SNJ (2006) A *Toxoplasma gondii* phosphoinositide phospholipase C (TgPI-PLC) with
1008 high affinity for phosphatidylinositol. *Biochem J* 394: 417-425.
- 1009 21. Bullen HE, Jia Y, Yamarlyo-Botte Y, Bisio H, Zhang O, et al. (2016) Phosphatidic Acid-Mediated Signaling Regulates
1010 Microneme Secretion in *Toxoplasma*. *Cell Host Microbe* 19: 349-360.
- 1011 22. Balestra AC, Koussis K, Klages N, Howell SA, Flynn HR, et al. (2021) Ca(2+) signals critical for egress and
1012 gametogenesis in malaria parasites depend on a multipass membrane protein that interacts with PKG. *Sci Adv*
1013 7.
- 1014 23. Lourido S, Tang K, Sibley LD (2012) Distinct signalling pathways control *Toxoplasma* egress and host-cell invasion.
1015 *EMBO J* 31: 4524-4534.

- 1016 24. McCoy JM, Whitehead L, van Dooren GG, Tonkin CJ (2012) TgCDPK3 regulates calcium-dependent egress of
1017 *Toxoplasma gondii* from host cells. PLoS Pathog 8: e1003066.
- 1018 25. Tagoe DNA, Drozda AA, Falco JA, Bechtel TJ, Weerapana E, et al. (2021) Ferlins and TgDOC2 in Toxoplasma
1019 Microneme, Rhoptry and Dense Granule Secretion. Life (Basel) 11.
- 1020 26. Long S, Brown KM, Drewry LL, Anthony B, Phan I, et al. (2017) Calmodulin-like proteins localized to the conoid
1021 regulate motility and cell invasion by *Toxoplasma gondii*. PloS Pathogens 13: e1006379.
- 1022 27. Jia Y, Marq JB, Bisio H, Jacot D, Mueller C, et al. (2017) Crosstalk between PKA and PKG controls pH-dependent host
1023 cell egress of *Toxoplasma gondii*. EMBO J 36: 3250-3267.
- 1024 28. Uboldi AD, Wilde ML, McRae EA, Stewart RJ, Dagley LF, et al. (2018) Protein kinase A negatively regulates Ca²⁺
1025 signalling in *Toxoplasma gondii*. PLoS Biol 16: e2005642.
- 1026 29. Brown KM, Tonkin CJ, Billker O, Sibley LD (2019) Calcium and cyclic nucleotide signaling networks in *Toxoplasma*
1027 *gondii*. In: Weiss LM, Kim K, editors. *Toxoplasma gondii: The Model Apicomplexan: Perspectives and Methods*.
1028 3rd ed: Academic Press. pp. in press.
- 1029 30. Hortua Triana MA, Marquez-Nogueras KM, Vella SA, Moreno SNJ (2018) Calcium signaling and the lytic cycle of the
1030 Apicomplexan parasite *Toxoplasma gondii*. Biochim Biophys Acta Mol Cell Res 1865: 1846-1856.
- 1031 31. Nagamune K, Sibley LD (2006) Comparative genomic and phylogenetic analyses of calcium ATPases and
1032 calcium-regulated proteins in the Apicomplexa. Molec Biol Evol 23: 1613-1627.
- 1033 32. Prole DL, Taylor CW (2011) Identification of intracellular and plasma membrane calcium channel homologues in
1034 pathogenic parasites. PLoS One 6: e26218.
- 1035 33. Thastrup O, Cullen PJ, Drobak BK, Hanley MR, Dawson AP (1990) Thapsigargin, a tumor promotor, discharges
1036 intracellular Ca²⁺ stores by specific inhibition of the endoplasmic reticulum Ca²⁺-ATPase. Proc Natl Acad Sci USA
1037 87: 2766-2470.
- 1038 34. Nagamune K, Moreno SNJ, Sibley LD (2007) Artemisinin resistant mutants of *Toxoplasma gondii* have altered calcium
1039 homeostasis. Anti Microb Agents Chemother 51: 3816-3823.
- 1040 35. Moreno SNJ, Zhong L (1996) Acidocalcisomes in *Toxoplasma gondii* tachyzoites. Biochemical Journal 313: 655-659.
- 1041 36. Luo S, Ruiz FA, Moreno SN (2005) The acidocalcisome Ca²⁺ ATPase (TgA1) of *Toxoplasma gondii* is required for
1042 polyphosphate storage, intracellular calcium homeostasis and virulence. Molec Micro 55: 1034-1045.
- 1043 37. Vella SA, Moore CA, Li ZH, Hortua Triana MA, Potapenko E, et al. (2021) The role of potassium and host calcium
1044 signaling in *Toxoplasma gondii* egress. Cell Calcium 94: 102337.
- 1045 38. Vella SA, Calixto A, Asady B, Li ZH, Moreno SNJ (2020) Genetic Indicators for Calcium Signaling Studies in *Toxoplasma*
1046 *gondii*. Methods Mol Biol 2071: 187-207.
- 1047 39. Lovett JL, Sibley LD (2003) Intracellular calcium stores in *Toxoplasma gondii* govern invasion of host cells. J Cell Sci
1048 116: 3009-3016.
- 1049 40. Sidik SM, Hortua Triana MA, Paul AS, El Bakkouri M, Hackett CG, et al. (2016) Using a Genetically Encoded Sensor to
1050 Identify Inhibitors of *Toxoplasma gondii* Ca²⁺ Signaling. J Biol Chem 291: 9566-9580.
- 1051 41. Borges-Pereira L, Budu A, McKnight CA, Moore CA, Vella SA, et al. (2015) Calcium Signaling throughout the
1052 *Toxoplasma gondii* Lytic Cycle: A STUDY USING GENETICALLY ENCODED CALCIUM INDICATORS. J Biol Chem 290:
1053 26914-26926.
- 1054 42. Brown KM, Lourido S, Sibley LD (2016) Serum Albumin Stimulates Protein Kinase G-dependent Microneme Secretion
1055 in *Toxoplasma gondii*. J Biol Chem 291: 9554-9565.
- 1056 43. Ferguson DJP, Hutchison WM, Pettersen E (1989) Tissue cyst rupture in mice chronically infected with *Toxoplasma*
1057 *gondii*. Parasitol Res 75: 599-603.
- 1058 44. Frenkel JK, Escajadillo A (1987) Cyst rupture as a pathogenic mechanism of toxoplasmic encephalitis. American
1059 Journal of Tropical Medicine and Hygiene 36: 517-522.
- 1060 45. Hofflin JM, Conley FK, Remington JS (1987) Murine model of intracerebral toxoplasmosis. Journal of Infectious
1061 Diseases 155: 550-556.
- 1062 46. Soète M, Fortier B, Camus D, Dubremetz JF (1993) *Toxoplasma gondii*: kinetics of bradyzoite-tachyzoite

- 1063 interconversion *in vitro*. Exp Parasitol 76: 259-264.
- 1064 47. Swierzy IJ, Luder CG (2015) Withdrawal of skeletal muscle cells from cell cycle progression triggers differentiation of
1065 Toxoplasma gondii towards the bradyzoite stage. Cell Microbiol 17: 2-17.
- 1066 48. Halonen SK, Lyman WD, Chiu FC (1996) Growth and development of *Toxoplasma gondii* in human neurons and
1067 astrocytes. J Neuropathology and Exp Neurology 55: 1150-1156.
- 1068 49. White MW, Radke JR, Radke JB (2014) Toxoplasma development - turn the switch on or off? Cell Microbiol 16:
1069 466-472.
- 1070 50. Beeler TJ, Jona I, Martonosi A (1979) The effect of ionomycin on calcium fluxes in sarcoplasmic reticulum vesicles
1071 and liposomes. J Biol Chem 254: 6229-6231.
- 1072 51. Lourido S, Shuman J, Zhang C, Shokat KM, Hui R, et al. (2010) Calcium-dependent protein kinase 1 is an essential
1073 regulator of exocytosis in Toxoplasma. Nature 465: 359-362.
- 1074 52. Cranfill PJ, Sell BR, Baird MA, Allen JR, Lavagnino Z, et al. (2016) Quantitative assessment of fluorescent proteins. Nat
1075 Methods 13: 557-562.
- 1076 53. Marquez-Nogueras KM, Hortua Triana MA, Chasen NM, Kuo IY, Moreno SN (2021) Calcium signaling through a
1077 transient receptor channel is important for Toxoplasma gondii growth. Elife 10.
- 1078 54. Nagamune K, Moreno SN, Chini EN, Sibley LD (2008) Calcium regulation and signaling in apicomplexan parasites.
1079 Subcell Biochem 47: 70-81.
- 1080 55. Maldonado EN, Lemasters JJ (2014) ATP/ADP ratio, the missed connection between mitochondria and the Warburg
1081 effect. Mitochondrion 19 Pt A: 78-84.
- 1082 56. Frenal K, Dubremetz JF, Lebrun M, Soldati-Favre D (2017) Gliding motility powers invasion and egress in Apicomplexa.
1083 Nat Rev Microbiol 15: 645-660.
- 1084 57. Carruthers VB (2019) Interrupting Toxoplasma's Regularly Scheduled Program of Egress. Trends Parasitol 35:
1085 338-340.
- 1086 58. Stasic AJ, Dykes EJ, Cordeiro CD, Vella SA, Fazli MS, et al. (2021) Ca(2+) entry at the plasma membrane and uptake by
1087 acidic stores is regulated by the activity of the V-H(+)-ATPase in Toxoplasma gondii. Mol Microbiol.
- 1088 59. Lemgruber L, Lupetti P, Martins-Duarte ES, De Souza W, Vommario RC (2011) The organization of the wall filaments
1089 and characterization of the matrix structures of Toxoplasma gondii cyst form. Cell Microbiol 13: 1920-1932.
- 1090 60. Tu V, Mayoral J, Sugi T, Tomita T, Han B, et al. (2019) Enrichment and Proteomic Characterization of the Cyst Wall
1091 from In Vitro Toxoplasma gondii Cysts. mBio 10.
- 1092 61. Zhang YW, Halonen SK, Ma YF, Wittner M, Weiss LM (2001) Initial characterization of CST1, a *Toxoplasma gondii* cyst
1093 wall glycoprotein. Infect Immun 69: 501-507.
- 1094 62. Tomita T, Bzik DJ, Ma YF, Fox BA, Markillie LM, et al. (2013) The Toxoplasma gondii cyst wall protein CST1 is critical for
1095 cyst wall integrity and promotes bradyzoite persistence. PLoS Pathog 9: e1003823.
- 1096 63. Tomita T, Sugi T, Yakubu R, Tu V, Ma Y, et al. (2017) Making Home Sweet and Sturdy: Toxoplasma gondii ppGalNAc-Ts
1097 Glycosylate in Hierarchical Order and Confer Cyst Wall Rigidity. mBio 8.
- 1098 64. Dubey JP (1998) Re-examination of resistance of *Toxoplasma gondii* tachyzoites and bradyzoites to pepsin and
1099 trypsin digestion. Parasitology 116: 43-50.
- 1100 65. Lin SS, Blume M, von Ahsen N, Gross U, Bohne W (2011) Extracellular Toxoplasma gondii tachyzoites do not require
1101 carbon source uptake for ATP maintenance, gliding motility and invasion in the first hour of their extracellular
1102 life. Int J Parasitol 41: 835-841.
- 1103 66. Blume M, Rodriguez-Contreras D, Landfear S, Fleige T, Soldati-Favre D, et al. (2009) Host-derived glucose and its
1104 transporter in the obligate intracellular pathogen Toxoplasma gondii are dispensable by glutaminolysis. Proc
1105 Natl Acad Sci U S A 106: 12998-13003.
- 1106 67. MacRae JJ, Sheiner L, Nahid A, Tonkin C, Striepen B, et al. (2012) Mitochondrial metabolism of glucose and
1107 glutamine is required for intracellular growth of Toxoplasma gondii. Cell Host Microbe 12: 682-692.
- 1108 68. Cardenas C, Miller RA, Smith I, Bui T, Molgo J, et al. (2010) Essential regulation of cell bioenergetics by constitutive
1109 InsP3 receptor Ca2+ transfer to mitochondria. Cell 142: 270-283.

- 1110 69. Gherardi G, Monticelli H, Rizzuto R, Mammucari C (2020) The Mitochondrial Ca(2+) Uptake and the Fine-Tuning of
1111 Aerobic Metabolism. *Front Physiol* 11: 554904.
- 1112 70. Pang X, Halaly T, Crane O, Keilin T, Keren-Keiserman A, et al. (2007) Involvement of calcium signalling in dormancy
1113 release of grape buds. *J Exp Bot* 58: 3249-3262.
- 1114 71. Steinhorst L, Kudla J (2013) Calcium - a central regulator of pollen germination and tube growth. *Biochim Biophys*
1115 *Acta* 1833: 1573-1581.
- 1116 72. Humeau J, Bravo-San Pedro JM, Vitale I, Nunez L, Villalobos C, et al. (2018) Calcium signaling and cell cycle:
1117 Progression or death. *Cell Calcium* 70: 3-15.
- 1118 73. Nance JP, Vannella KM, Worth D, David C, Carter D, et al. (2012) Chitinase dependent control of protozoan cyst
1119 burden in the brain. *PLoS Pathog* 8: e1002990.
- 1120 74. Nadipuram SM, Thind AC, Rayatpisheh S, Wohlschlegel JA, Bradley PJ (2020) Proximity biotinylation reveals novel
1121 secreted dense granule proteins of *Toxoplasma gondii* bradyzoites. *PLoS One* 15: e0232552.
- 1122 75. Dzierszinski F, Nishi M, Ouko L, Roos DS (2004) Dynamics of *Toxoplasma gondii* differentiation. *Eukaryot Cell* 3:
1123 992-1003.
- 1124 76. Tobin CM, Knoll LJ (2012) A patatin-like protein protects *Toxoplasma gondii* from degradation in a nitric
1125 oxide-dependent manner. *Infect Immun* 80: 55-61.
- 1126 77. Wang ZT, Harmon S, O'Malley KL, Sibley LD (2015) Reassessment of the role of aromatic amino acid hydroxylases and
1127 the effect of infection by *Toxoplasma gondii* on host dopamine. *Infect Immun* 83: 1039-1047.
- 1128 78. Carruthers VB, Giddings OK, Sibley LD (1999) Secretion of micronemal proteins is associated with *Toxoplasma*
1129 invasion of host cells. *Cell Microbiol* 1: 225-236.
- 1130 79. Alaganaan A, Fentress SJ, Tang K, Wang Q, Sibley LD (2013) *Toxoplasma* GRA7 effector increases turnover of
1131 immunity-related GTPases and contributes to acute virulence in the mouse. *Proc Natl Acad Sci (USA)* 111:
1132 1126-1131.
- 1133 80. Shen B, Brown K, Long S, Sibley LD (2017) Development of CRISPR/Cas9 for Efficient Genome Editing in *Toxoplasma*
1134 *gondii*. *Methods Mol Biol* 1498: 79-103.
- 1135 81. Shen B, Brown KM, Lee TD, Sibley LD (2014) Efficient gene disruption in diverse strains of *Toxoplasma gondii* using
1136 CRISPR/CAS9. *mBio* 13;5(3):e01114-14.
- 1137 82. Livak KJ, Schmittgen TD (2001) Analysis of relative gene expression data using real-time quantitative PCR and the
1138 2(-delta-delta C(T)) method. *Methods* 25: 402-408.
- 1139 83. Menegollo M, Tessari I, Bubacco L, Szabadkai G (2019) Determination of ATP, ADP, and AMP Levels by
1140 Reversed-Phase High-Performance Liquid Chromatography in Cultured Cells. *Methods Mol Biol* 1925: 223-232.
1141